nature plants

ARTICLES

https://doi.org/10.1038/s41477-021-01002-z

Check for updates

A photoregulatory mechanism of the circadian clock in *Arabidopsis*

Xu Wang[1,2,3], Bochen Jiang[2,3], Lianfeng Gu[1,3], Yadi Chen[1], Manuel Mora[2], Mulangma Zhu[2], Eliace Noory[2], Qin Wang[1]✉ and Chentao Lin[2]✉

Cryptochromes (CRYs) are photoreceptors that mediate light regulation of the circadian clock in plants and animals. Here we show that CRYs mediate blue-light regulation of N^6-methyladenosine (m^{6}A) modification of more than 10% of messenger RNAs in the *Arabidopsis* transcriptome, especially those regulated by the circadian clock. CRY2 interacts with three subunits of the METTL3/14-type N^6-methyladenosine RNA methyltransferase (m^{6}A writer): MTA, MTB and FIP37. Photo-excited CRY2 undergoes liquid–liquid phase separation (LLPS) to co-condense m^{6}A writer proteins in vivo, without obviously altering the affinity between CRY2 and the writer proteins. *mta* and *cry1cry2* mutants share common defects of a lengthened circadian period, reduced m^{6}A RNA methylation and accelerated degradation of mRNA encoding the core component of the molecular oscillator circadian clock associated 1 (CCA1). These results argue for a photoregulatory mechanism by which light-induced phase separation of CRYs modulates m^{6}A writer activity, mRNA methylation and abundance, and the circadian rhythms in plants.

Organisms respond to daily light–dark cycles via the coordinated actions of photoreceptors and the circadian clock[1–3]. Photoreceptors mediate light entrainment of the circadian clock by regulating the abundance and activity of core components of the molecular oscillator to sustain the circadian phase and period lengths of ~24 h. Plant and insect CRYs act as photoreceptors to mediate photo-entrainment of the molecular oscillator, whereas mammalian CRYs act as the light-independent core component of the molecular oscillator[4–6]. How photoreceptors mediate photo-entrainment of the circadian clock is not fully understood. For example, plant photoreceptors, including phytochrome A, phytochrome B, cryptochrome 1 (CRY1) and cryptochrome 2 (CRY2) mediate photo-entrainment of the circadian clock by regulating messenger RNA transcription[1]. mRNA abundance is determined by not only mRNA synthesis, but also mRNA degradation[7], yet involvement of the latter in photo-entrainment is largely unexplored. It has been shown that m^{6}A methylation of mRNAs regulates the circadian clock[8–10] and the stability of mRNAs[11,12], but whether or how photoreceptors mediate light regulation of mRNA methylation or stability to control the circadian clock is not known.

CRYs mediate blue-light regulation of m^{6}A epitranscriptome

Because m^{6}A is the most abundant internal mRNA modification[13–15], we analysed m^{6}A epitranscriptomes and transcriptomes in *Arabidopsis* wild-type (WT) and *cry1cry2* mutant seedlings grown in darkness or in continuous blue light, using m^{6}A methyl-RNA immunoprecipitation and RNA sequencing (m^{6}A-seq) and conventional RNA-seq methods (Fig. 1a)[16]. We identified the transcriptomes and m^{6}A-bearing epitranscriptomes of 21,817 and 8,877 genes, respectively ($P<0.01$, false discovery rate <0.01; Supplementary Table 1). The m^{6}A-bearing mRNAs detected in this study show 70–93% overlap with that of five *Arabidopsis* epitranscriptomes reported previously (Supplementary Table 1), confirming the high reproducibility of the m^{6}A-seq approach. In comparison with WT seedlings grown in blue light, the *cry1cry2* mutant exhibits ~45% reduction ($P<2.141\times10^{-5}$) in the overall size of the m^{6}A epitranscriptome and a massive decrease in relative m^{6}A abundance in mRNA (Extended Data Fig. 1 and Supplementary Table 1). Plotting binary logarithms of the blue light/dark (B/D) ratios of m^{6}A reads against those of the respective transcripts reveals a positive correlation between photoresponsive changes in the overall epitranscriptomes and transcriptomes in WT plants (Fig. 1b), as well as that of individual Gene Ontology (GO) groups such as clock-controlled genes (CCG) (Fig. 1c and Extended Data Fig. 2). Namely, a greater change in m^{6}A abundance in response to blue light correlates with a greater change in transcript abundance and vice versa. This correlation is diminished in the *cry1cry2* mutant (Fig. 1b,c, Pearson correlation $r=0.7$ in WT, $r=0.3$ in *cry1cry2*). The CRY-dependent change in m^{6}A abundance may be due to changes in RNA abundance or/and changes in RNA methylation, so we examined how blue light and the *cry1cry2* mutation affect the density of m^{6}A markers along individual transcripts, by mapping the binary logarithms of B/D ratios of m^{6}A density to individual transcripts (Fig. 1d,e and Extended Data Fig. 2). This analysis demonstrates that m^{6}A density changes show a clear CRY-dependent photoresponse, especially in the 3′ untranslated regions (UTR) of the epitranscriptomes. CRY-mediated photoregulation of m^{6}A RNA methylation is better shown by m^{6}A density maps of individual mRNAs, such as those encoding photoreceptors (Fig. 1f), m^{6}A writer proteins (Fig. 1g) and central oscillator genes (COGs) (Fig. 1h). These results suggest that CRY-dependent RNA methylation may have a role in signalling or feedback modes to sustain photochronological control of RNA metabolism[1,4]. m^{6}A methylations have been detected in the transcripts of ten known COGs, including *CCA1* that encodes a key component of the molecular oscillator in *Arabidopsis*[17], and RNA deposition of those transcripts decreased markedly in light-grown *cry1cry2* mutant plants in comparison with WT plants (Fig. 1h and Extended Data Fig. 1b). CCGs are consistently enriched non-proportionally in the m^{6}A epitranscriptome (Fig. 1i and Supplementary Table 1).

[1]Basic Forestry and Proteomics Research Center, Fujian Agriculture and Forestry University, Fuzhou, China. [2]Department of Molecular, Cell and Developmental Biology, University of California, Los Angeles, CA, USA. [3]These authors contributed equally: Xu Wang, Bochen Jiang, Lianfeng Gu. ✉e-mail: qinwangcry@163.com; clin@mcdb.ucla.edu

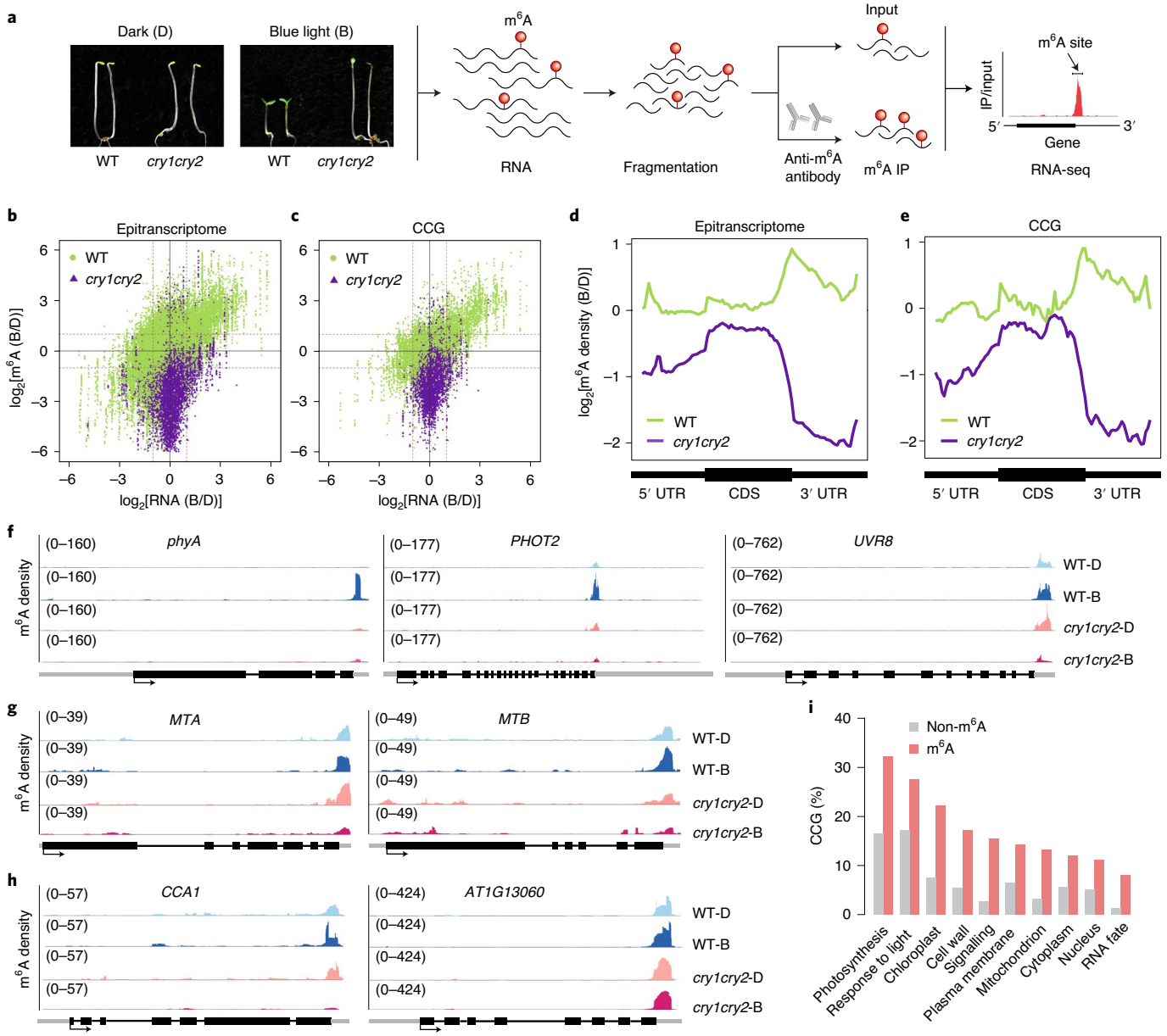

Fig. 1 | CRYs mediate blue-light regulation of epitranscriptomes. a, Diagram showing the m^{6}A-seq assay in this study. WT and *cry1cry2* seedlings grown in the dark or in continuous blue light (30 μmol m^{-2} s^{-1}) for 6 days were harvested for RNA isolation. The fragmentated RNA was either saved as the 'Input' sample or used for immunoprecipitation (IP) with anti-m^{6}A antibodies. Input and IP samples from three independent experiments were sequenced in parallel. **b**,**c**, Scatter plots showing photoresponsive changes in m^{6}A and transcript abundance for the epitranscriptome (**b**) or CCG (**c**) of the indicated genotypes. log$_2$[m^{6}A (B/D)] is calculated from the ratio of fold changes (FC) in normalized m^{6}A reads for light- and dark-grown samples (B/D). log$_2$[RNA (B/D)] is calculated from the ratio of FC in fragments per kilobase of transcript per million mapped reads for light- and dark-grown samples (B/D). **d**,**e**, Photoresponsive m^{6}A density changes in the genome-wide epitranscriptome (**d**) or CCG (**e**). log$_2$[m^{6}A density (B/D)] is calculated from the ratio of m^{6}A density between light- and dark-grown (B/D) samples of the indicated genotypes. **f**–**h**, Genomic visualization of m^{6}A density maps of representative photoreceptor genes (*phyA, PHOT2* and *UVR8*) (**f**), m^{6}A writer genes (*MTA* and *MTB*) (**g**) and core circadian clock gene *CCA1* (**h**) in WT and *cry1cry2* seedlings grown in the dark (D) or in blue light (B). *AT1G13060* is an arbitrarily selected gene that shows no change in density among different samples (**h**). Gene structures are displayed below the m^{6}A density map with the UTR (grey box), exon (black box) and intron (black line) shown. Arrows indicate the direction of transcription. **i**, Differential enrichment of CCG among m^{6}A-modified or unmodified transcripts of the indicated GO categories.

For example, approximately 11–22% of m^{6}A-modified mRNAs encoding nuclear, cytoplasmic, chloroplast or mitochondrial proteins are classified as CCGs, more than twice the proportion of CCGs identified in unmodified mRNAs encoding the respective proteomes (3–7%). These results prompt us to investigate the hypothesis that CRYs may mediate blue-light regulation of m^{6}A RNA methylation to affect mRNA abundance and the circadian clock.

Light-independent and light-dependent behaviours of the CRY2/writer complex

We tested the above hypothesis by investigating physical interactions between CRY2 and the m^{6}A methyltransferase (writer), because proteins associated with the functions of m^{6}A RNA methylation were among putative CRY2-associated proteins identified in our CRY2 immunoprecipitation mass spectrometry (IP–MS)

surveys[18]. It has been reported previously that the *Arabidopsis* m^{6}A writer proteins, MTA, MTB and FIP37, are counterparts of the key subunits of the metazoan METTL3/14-type m^{6}A writer, METTL3, METTL14 and WTAP, respectively[13,15,19], and that MTA, MTB and FIP37 are essential for m^{6}A mRNA methylation in *Arabidopsis*[15,20,21]. In heterologous human embryonic kidney 293T (HEK293T) cells, CRY2 interacts with all three METTL3/14-type m^{6}A writer proteins, MTA, MTB and FIP37, although no obvious light response was detected using co-immunoprecipitation assays (Extended Data Fig. 3). The seemingly light-independent formation of the CRY2/MTA and CRY2/FIP37 complexes is also detected in *Arabidopsis* seedlings (Fig. 2c,d). A modestly decreased co-immunoprecipitation signal of CRY2 detected in seedlings exposed to 15 min of strong (100 μmol m^{-2} s^{-1}) blue light (Fig. 2b) most likely results from blue light-induced CRY2 degradation[22,23]. We found that human CRY2 (hCRY2) also forms a complex with the human METTL3/14 m^{6}A writer proteins, including METTL3, METTL14 and WTAP in HEK293 cells (Fig. 2e,f), suggesting possible evolutionary conservation of interactions between CRYs and the writer proteins in plants and Metazoa. We then examined in more detail the interaction between CRY2 and MTA, which is the *Arabidopsis* counterpart of the catalytic subunit of mammalian m^{6}A writer METTL3. Consistent with the light-independent interaction of CRY2 and MTA detectable in co-immunoprecipitation assays (Fig. 2a), the flavin adenine dinucleotide (FAD)-deficient mutant CRY2D387A[24,25] also interacts with MTA (Extended Data Fig. 3d). We further analysed the domain relationship between CRY2 and MTA. CRYs have two domains, the photolyase homologous region (PHR) domain that binds to the chromophore FAD and the CRY C-terminal extension (CCE) domain, which is an intrinsically disordered region[4]. The C-terminal domain of MTA is highly homologous (~70% similar) with the methyltransferase domain (MTase) of human METTL3, whereas the N-terminal domain of MTA and METTL3 share little similarity. Both the PHR and CCE domains of CRY2 interact with MTA (Fig. 2a), and both the C-terminal MTase domain and N-terminal domain of MTA interact with the PHR domain of CRY2 (Fig. 2b). It is highly improbable that all the stable co-immunoprecipitation complexes detected result from non-specific promiscuous bindings. Rather, it seems more plausible that CRY2 interacts with the m^{6}A writer complex via multivalent interactions, including weak non-covalent bonds involving different domains of CRY2, different domains of the writer protein and different subunits of the writer complex (Fig. 2g). Consistent with this proposition, blue light clearly inhibits the interaction between the PHR domain of CRY2 and the MTase domain of MTA (Fig. 2b). This suggests that the CRY2/writer complex may undergo photoresponsive structural rearrangements in vivo, by altering various non-covalent bonds involved in the multivalent interaction of CRY2 and writer proteins. For example, light may suppress interactions between the PHR domain of CRY2 and the MTase domain of MTA but stimulate interactions between the CCE domain of CRY2 and the N-terminal non-MTase domain of MTA in the native environment of the full-length proteins. This scenario can explain the lack of a light response for interactions between full-length proteins (Fig. 2a, c) but clear light response for interactions between fragments of CRY2 and MTA (Fig. 2b).

We further examined the possible photoresponses of the CRY2/writer complexes using a bimolecular fluorescence complementation (BiFC) assay[26] in *Arabidopsis* protoplasts. In the absence of CRY2 co-expression, MTA, MTB and FIP37 proteins all exhibit uniform distribution in the nucleoplasm (Fig. 2h,j). However, when CRY2 and these writer proteins are co-expressed as BiFC pairs in light-treated protoplasts, the reconstituted yellow fluorescent protein (YFP) fluorescence resulting from physical interaction between the respective BiFC pairs of CRY2–nYFP and MTA–cYFP, CRY2–nYFP and MTB–cYFP, or CRY2–nYFP and FIP37–cYFP (nYFP and cYFP are the N- and C-terminal fragments of YFP, respectively) is mostly detected in discrete nuclear speckles that resemble the CRY2 photobody[26–28] (Fig. 2i, upper, and Fig. 2j). Subcellular co-localization assays indicate that the nuclear speckles of CRY2/writer complexes coincide with the CRY2 photobody (Extended Data Fig. 4). In the control experiment, the photo-insensitive CRY2^{D387A}–nYFP mutant still interacts with MTA–cYFP, as indicated by the reconstituted YFP fluorescence (Fig. 2i, lower, and Fig. 2j), which is consistent with the light-independent interaction of CRY2 and MTA (Fig. 2a). Importantly, BiFC signals of the CRY2^{D387A}–nYFP/MTA–cYFP complex distribute uniformly in the nucleoplasm but not in the photobody (Fig. 2i, lower, Fig. 2j and Supplementary Video 1), which is consistent with the light-insensitive nature of the CRY2^{D387A} mutant[24,25]. We reasoned that light may induce co-condensation of CRY2 and MTA in photobodies without changing the overall affinity between CRY2 and MTA. To test this proposition, we compared the BiFC signal of CRY2–nYFP and MTA–cYFP fusion proteins co-expressed in *Arabidopsis* protoplasts kept in the dark or exposed to blue light (Fig. 2k,l). BiFC fluorescence signals resulting from interactions of CRY2–nYFP and MTA–cYFP were examined after excitation of YFP with a 514 nm laser, with or without the prior photo-activation of CRY2 by blue light (488 nm). In protoplasts kept in the dark, the BiFC signal of reconstituted YFP fluorescence was distributed uniformly in the nucleoplasm (Fig. 2k, upper; 0 s). However, within 3 s after blue light (488 nm) exposure, BiFC signals of the CRY2–nYFP/MTA–cYFP complex were detected mostly

Fig. 2 | Multivalent interaction of the CRY2/writer complex. a, Co-immunoprecipitation assays showing interactions between MTA and CRY2 or CRY2 fragments in HEK293T cells. BL, blue light (100 μmol m^{-2} s^{-1}). Two independent experiments show similar results. **b**, Co-immunoprecipitation assays showing the interactions between CRY2^{N489} and MTA or MTA fragments in HEK293T cells. BL, blue light (100 μmol m^{-2} s^{-1}). Two independent experiments show similar results. **c,d**, Co-immunoprecipitation assay showing CRY2/MTA (**c**) or CRY2/PIF37 (**d**) complexes in *Arabidopsis*. BL, blue light (30 μmol m^{-2} s^{-1}). Two independent experiments show similar results. **e**, Co-immunoprecipitation assays showing interactions between hCRY2 and m^{6}A writers in HEK293T cells. Two independent experiments show similar results. **f**, Co-immunoprecipitation assays showing interactions between METTL3 and different hCRY2 domains. Two independent experiments show similar results. **g**, Left: diagram depicting the multivalent interactions of CRY2 and MTA. The circle in the centre of an arch indicates the full-length protein. Coloured links indicate direct interactions between the domains. Right: comparison of *Arabidopsis* and human CRY/writer complexes. Coloured and grey links indicate interactions detected in this study and the literature, respectively. **h**, Subcellular distributions of MTA-YFP, MTB-YFP and FIP37-YFP in *Arabidopsis* protoplasts. The dashed circle outlines the protoplast, a zoomed in view of the nucleus is shown in the lower panel. Scale bar, 2 μm. **i**, BiFC assays showing interactions of CRY2/MTA, CRY2/MTB and CRY2/FIP37 in *Arabidopsis* protoplasts under blue light. CRY2^{D387A} mutant is used as the negative control. Scale bar, 2 μm. **j**, Quantification of partition coefficient of YFP signals of writer-YFP fusion proteins or co-participation coefficient of BiFC signals of CRY2/writer complexes from the experiments shown in (**i**) and (**h**), respectively (mean ± s.d.; $n = 18$ measurements from five cells). **k**, Time-lapse images showing BiFC signals of CRY2/MTA and CRY2^{D387A}/MTA complex in response to blue light. Scale bar, 2 μm. **l**, Co-partition coefficient of CRY2/MTA or CRY2^{D387A}/MTA complex from the assay shown in (**k**) (mean ± s.d.; $n = 15$ measurements from three nuclei). **m**, Fluorescence recovery of CRY2/MTA BiFC signals in FRAP assay. The double exponential fit (dark line) of averaged recovery curves is shown (mean ± s.e.m.; $n = 5$ independent FRAP experiments).

in the CRY2 photobodies (Fig. 2k, upper; 3 s). The co-partition coefficient of the BiFC signals, which measures the relative abundance of the CRY2–nYFP/MTA–cYFP complex in the CRY2 photobody, increased by ~400% within 30 s of blue-light illumination (Fig. 2l). By contrast, the mutant CRY2^{D387A}–nYFP/MTC–cYFP complex remained uniformly distributed throughout the nucleoplasm regardless of light treatment (Fig. 2k, lower, Fig. 2l), consistent with both the light-insensitive nature of the CRY2^{D387A} mutant[24,25] (Extended Data Fig. 3d) and light-independent interaction of CRY2 and MTA (Fig. 2a). As expected, no light-induced co-partition in photobodies was observed for the mutant CRY2^{D387A}–nYFP and MTA–cYFP BiFC proteins (Fig. 2l). CRY1 also interacts with MTA (Extended Data Fig. 3e). These results are consistent with the hypothesis that CRY1 and CRY2 act redundantly to regulate mRNA methylation in *Arabidopsis*. Together, these results argue that light promotes recruitment of the CRY/MTA complex into the CRY photobody without increasing the overall affinity between CRY and MTA proteins. Light-induced co-condensation may increase local

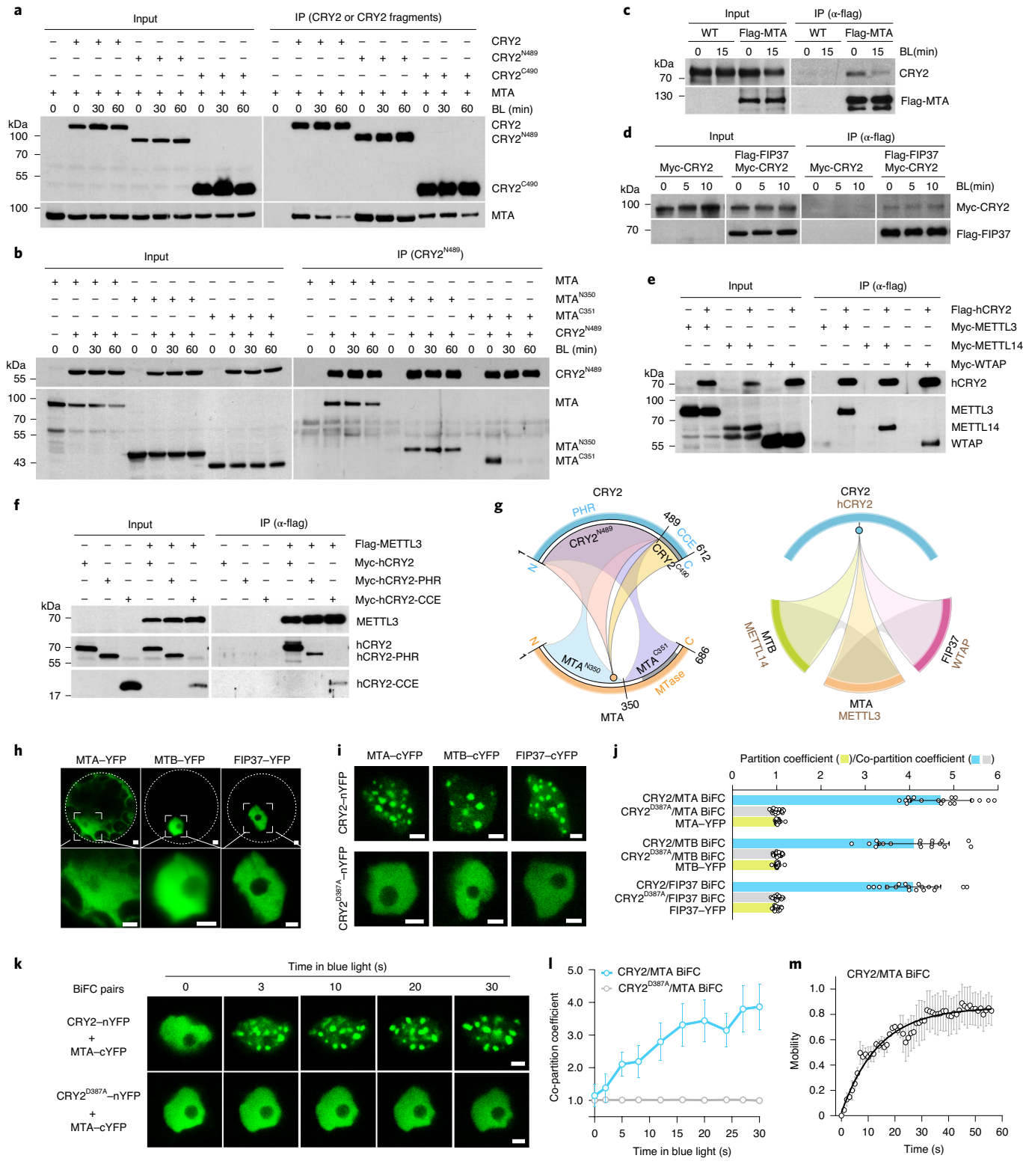

concentrations of the CRY/MTA complex within the CRY photobody, at the expense of the MTA concentration outside the CRY photobody. This mechanism may allow light regulation of RNA methylation without altering the overall stoichiometry or cellular concentration of the CRY/MTA complex.

Blue light induces liquid–liquid phase separation of CRY2 and the CRY2/MTA complex

CRY2 photobodies are blue light-induced CRY2 complexes observed for not only CRY2 fused to various fluorescent proteins, but also endogenous CRY2, and formation of CRY2 photobodies is integral to the photoresponsive function of CRY2[26–28]. The PHR domain of CRY2 and light-clustering proteins fused to various other proteins have been shown to drive light-induced liquid–liquid phase separation (LLPS)[29–31]. However, whether light can induce LLPS of a photoreceptor holoprotein in its native environment has not been reported. We reasoned that the multivalent nature of the interaction of CRY2 and MTA (Fig. 2a,b), the unusual photoresponsive domain relationship (Fig. 2a–g) and photoresponsive enrichment of the CRY2/MTA complex in the photobody (Fig. 2k–m) may be explained by photoresponsive LLPS of the CRY2 photobody. We tested whether CRY2 undergoes blue light-induced LLPS in vivo using four independent experiments, demonstrating that CRY2 photobodies have the hallmarks of light-induced LLPS[32,33], such as sphericity, mobility, fusibility and reversibility (Fig. 3, Extended Data Figs. 5–7 and Supplementary Videos 1 and 3). First, CRY2–green fluorescent protein (GFP) expressed in transgenic plants developed photobodies that are spherical droplets with a circularity and aspect ratio of ~1 (Fig. 3a,b and Supplementary Video 1). Second, photobleached CRY2–GFP photobodies recovered rapidly (within 30–40 s) in fluorescence recovery after photobleaching (FRAP) assays, indicating that CRY2–GFP photobodies are composed of condensed but highly mobile CRY2–GFP molecules (Fig. 3c, Extended Data Fig. 5a and Supplementary Video 2). Third, CRY2–DsRed (*Discosoma* sp. RFP) transiently expressed in *Arabidopsis* protoplasts formed photobodies in a wavelength-specific and dark-reversible manner (Fig. 3d, Extended Data Figs. 6 and 7 and Supplementary Video 3). In the fourth experiment, we analysed CRY2–YFP transiently expressed in *Arabidopsis* protoplasts because the CRY2–YFP photobodies are relatively easier to quantify under green excitation (514 nm) subsequent to activation of CRY2 by blue light (488 nm). Formation of CRY2–YFP photobodies was FAD- and blue light-dependent (Fig. 3e, Extended Data Figs. 4 and 5 and Supplementary Video 1); CRY2–YFP molecules condensed in photobodies were highly mobile (Fig. 3n and Extended Data Fig. 5b,c); smaller CRY2–YFP photobodies rapidly fused into larger ones (Fig. 3f); and formation of CRY2–YFP photobodies was inhibited by the LLPS inhibitor 1,6-hexanediol (Fig. 3g). These results argue that CRY2 undergoes blue light-induced LLPS in vivo.

CRY2–YFP expressed in heterologous HEK293T cells also formed photobody-like structures (Fig. 3h); however, these appear not to be present in the liquid phase. In comparison with CRY2 photobodies in plant cells, the photobody-like structures of CRY2–YFP in HEK293T cells exhibited markedly lower structural sphericity and molecular mobility (Fig. 3i,j and Extended Data Fig. 8). We had previously shown that blue light-specific phosphorylation of CRY2 is required for its function[18,34,35], and that CRY2 phosphorylation is catalysed by photoregulatory protein kinases (PPKs) in plant cells or heterologous HEK293T cells[18]. We reasoned that phosphorylation might be required to keep CRY2 photobodies in the liquid phase to avoid non-liquid phase aggregation and inactivation of the highly condensed CRY2 in vivo. We tested this hypothesis using the FRAP assay. Indeed, CRY2–YFP co-expressed with PPK1 in HEK293T cells formed photobodies with structural circularity and molecular mobility comparable with that of the CRY2–GFP or CRY2–YFP photobodies observed in vivo, whereas CRY2–YFP co-expressed with the catalytically inactive PPK1^{D267N} mutant[18] shows significantly ($P < 10^{-8}$) lower liquidity in the photobody-like structures (Fig. 3i,j and Extended Data Fig. 8). These results indicate that phosphorylation is not required for the photoresponsive condensation of CRY2, but it is required to maintain CRY2 condensates in the liquid phase. Like phosphorylation, the intrinsically disordered CCE domain of CRY2 (Fig. 3k) is also not required for CRY2 condensation but it is required to maintain the CRY2 photobody in the liquid phase (Fig. 3l–n and Extended Data Fig. 9). Importantly, the light-induced rapid (30–40 s) co-condensation of the CRY2/MTA complex is also found in the liquid phase in vivo, because BiFC signals resulting from interacting CRY2 and MTA molecules in the photobody exhibit mobility (Fig. 2m and Extended Data Fig. 4f) that is indistinguishable from that of the CRY2 molecules (Fig. 3c and Extended Data Fig. 5c). Taken together, these results support the hypothesis that photo-excited CRY2 undergoes LLPS to concentrate the CRY2/writer complex in the condensed liquid phase, or to bring the METTL3/14-type m^{6}A writer proteins to the appropriate subnuclear foci, and facilitate mRNA methylation in light-grown plants.

CRYs and MTA suppress period lengthening of the circadian clock and degradation of the *CCA1* mRNA

We next examined how the *mta* and *cry1cry2* mutations affect circadian rhythmicity, using the *pCCA1::LUC* and *pTOC1::LUC* luciferase reporters driven by the promoter of the COGs *CCA1* and *TOC1*, respectively[36,37]. Because *Arabidopsis* loss-of-function *mta* mutants are embryonically lethal[21,38], we prepared and analysed

Fig. 3 | Blue light elicits LLPS of CRY2. a, Droplet-like CRY2 photobodies in plant cells. Arrows indicate the same CRY2 photobody observed in the bright field or GFP channel. Scale bar, 5 μm. Four independent experiments showed similar results. **b**, Circularity and aspect ratio of CRY2 photobodies in plant cells (mean ± s.d.; $n = 166$ measurements from ten nuclei). **c**, FRAP assays of CRY2–GFP photobodies in plants. The double exponential fit (dark line) of averaged recovery curves is shown (mean ± s.d.; $n = 5$ independent FRAP experiments). **d**, Reversibility of CRY2–DsRed photobodies in *Arabidopsis* protoplasts indicated by the partition coefficient (mean ± s.d.; $n = 12$ measurements from three nuclei). Blue, light on; grey, light off. **e**, Partition coefficient of CRY2–YFP photobody formation in protoplasts. CRY2^{D387A}–YFP was used as the negative control (mean ± s.d.; $n = 15$ measurements from five nuclei). **f**, Fusion of CRY2–YFP photobodies in protoplasts, presented as either time-lapse images or a kymograph. Scale bar, 1 μm. Two independent experiments show similar results. **g**, 1,6-Hexanediol inhibits formation of CRY2–YFP photobodies in protoplasts. Scale bar, 2 μm. **h**, PPK1-dependent phosphorylation is not required for CRY2 photobody formation in HEK293T cells. Scale bar, 5 μm. Two independent experiments showed similar results. **i**, Circularity of CRY2–YFP photobodies from the assay presented in (**h**). D267N, PPK1^{D267N} mutant (mean ± s.d.; $n = 190$; *P* value, two-tailed Student's *t*-test). **j**, FRAP of CRY2–YFP photobodies in HEK293T cells. The double exponential fit (dark line) of averaged recovery curves is shown (mean ± s.d.; $n = 5$ independent FRAP experiments). **k**, Diagrams showing fragments in the PHR and CCE domain of CRY2. The disorder tendency of CRY2 is predicted by VL3 (blue) or VSL2B (grey) algorithms. **l**, The PHR domain mediates photobody condensation of CRY2. Fluorescence images of CRY2 and CRY2 fragments in HEK293T cells (scale bar, 5 μm) or nuclear localized CRY2 fragments in *Arabidopsis* protoplasts (scale bar, 2 μm) are shown. The dashed white circle outlines the nucleus in the cell. Five independent experiments showed similar results. **m**,**n**, FRAP assays performed in HEK293T cells (**m**) or *Arabidopsis* protoplasts (**n**). Double exponential fits (solid lines) of averaged recovery curves are shown (mean ± s.d.; $n = 5$ independent FRAP experiments). DIC, differential interference contrast.

luciferase reporter lines in a partially rescued *mta* mutant background (*ABI3::MTA/mta*, Extended Data Fig. 10) known to be markedly impaired in the m^{6}A epitranscriptome[11,38]. As reported previously, young seedlings of this *mta* mutant line exhibit no obvious phenotypic abnormality (Fig. 4a), but adult mutant plants are semi-dwarf with shorter and bushy bolts (Extended Data Fig. 10b)[11,38]. As expected, m^{6}A deposition of the *CCA1* mRNA exhibited a marked reduction in both *cry1cry2* and *mta* seedlings grown in blue light (Fig. 4b). Importantly, the *mta* mutant has a significantly ($P < 1.7 \times 10^{-5}$) lengthened circadian period under free-running conditions illuminated by continuous white light (90 μmol m^{-2} s^{-1}), resembling the long-period phenotype of the *cry1cry2* mutant (Fig. 4c)[36,37]. This demonstrates that MTA and CRYs are both required to suppress period lengthening of the circadian clock in light. We next compared how blue-light intensity affects the long-period phenotype of the two mutants. In this experiment, seedlings grown under a 12 h white light/12 h dark photoperiod were transferred to continuous blue light of various intensities (up to 40 μmol m^{-2} s^{-1}) to measure the circadian rhythm of the *pCCA1::LUC* reporter (Fig. 4d,e). In contrast to *cry1cry2*, which shows strong period

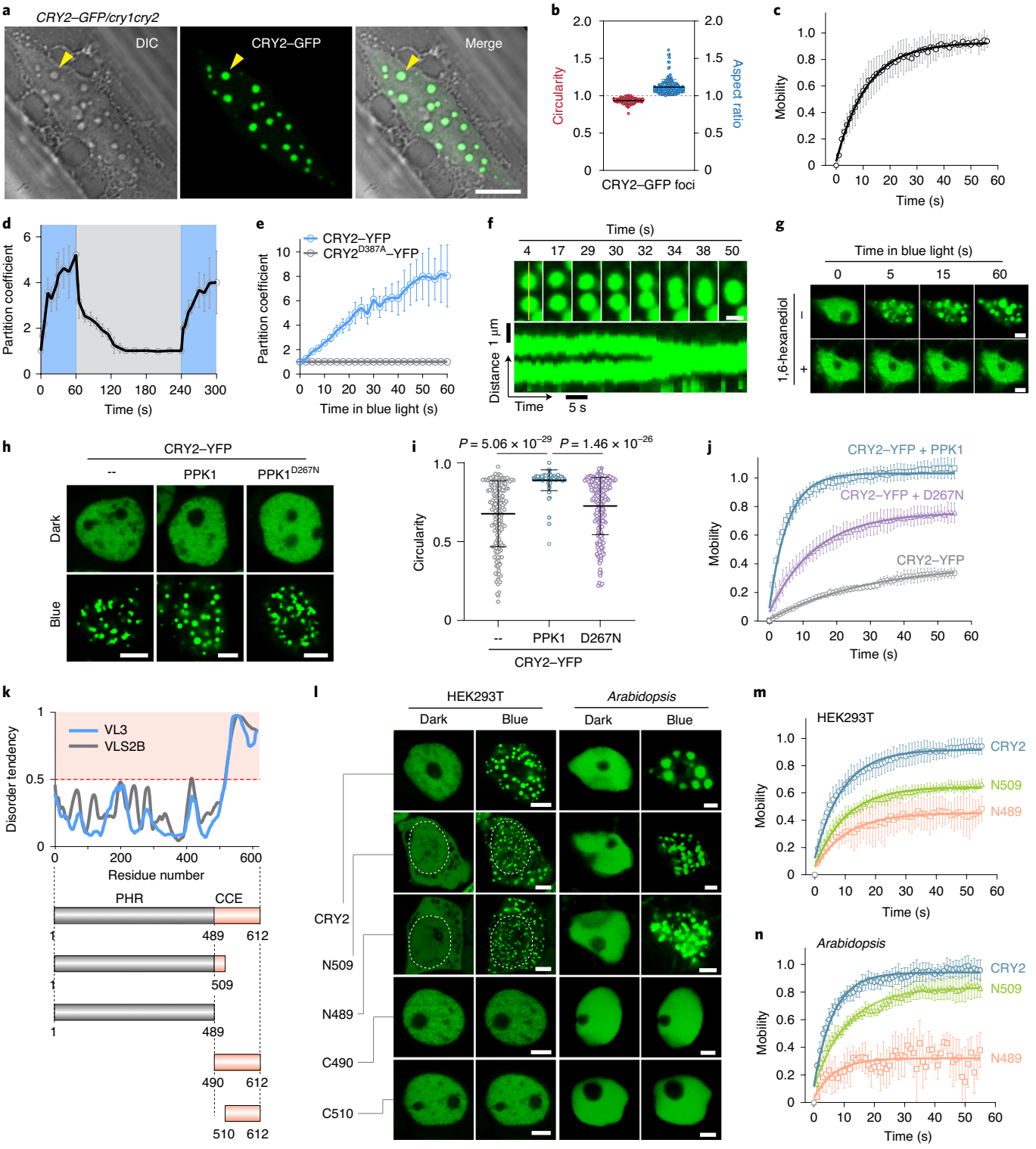

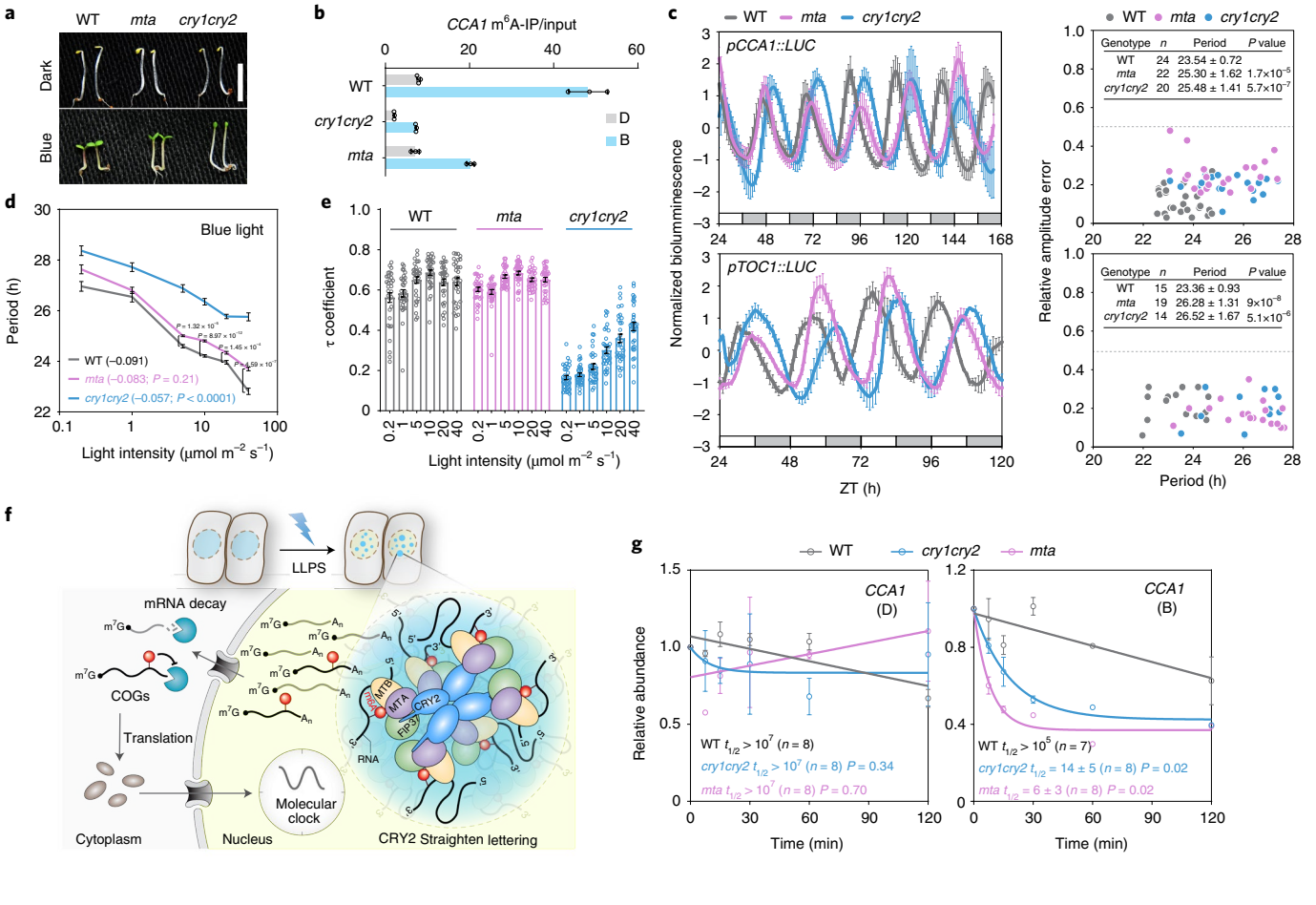

Fig. 4 | CRYs and MTA regulate *CCA1* mRNA metabolism and the circadian clock. a, Four-day-old seedlings of the indicated genotypes grown in the dark or in blue light (30 μmol m^{-2} s^{-1}). Scale bar, 1 cm. **b**, m^6A-immunoprecipitation–qPCR assays showing the relative abundance of m^6A on the 3′ UTR of *CCA1* mRNA in different genotypes in the dark (D) or blue light (B, 30 μmol m^{-2} s^{-1}). Values are given as mean ± s.d. ($n = 3$ independent experiments). **c**, Free-running rhythms of clock reporter lines in continuous white light (90 μmol m^{-2} s^{-1}). Normalized bioluminescence (mean ± s.e.m.; $n = 11$ seedlings for WT, $n = 10$ seedlings for *cry1cry2* and *mta* from two independent experiments) is shown. The correlation of relative amplitude error and period length is plotted. Statistical data are shown in the inset (period: mean ± s.d.; *P* value, two-tailed Student's *t*-test). **d**, Fluence response curve of *pCCA1::LUC* reporter lines in blue light (mean ± s.e.m.; *n* for WT under fluence rates from 0.2 to 40 μmol m^{-2} s^{-1} is 25, 24, 23, 22, 22 and 23; *n* for *cry1cry2* is 22, 25, 21, 21, 22 and 22; *n* for *mta* is 26, 26, 23, 24, 24 and 24 from three independent experiments; *P* value, two-tailed Student's *t*-test). Slopes of the best fitted linear regression of curves and the *P* value (*F* test) of slopes between WT and mutants are shown in parentheses. **e**, Rhythmicity tests of the *pCCA1::LUC* reporter lines under various intensities of blue light. The τ coefficient is shown as mean ± s.e.m. ($n = 32$ seedlings from three independent experiments). **f**, qPCR assays showing mRNA decay kinetics of *CCA1* in indicated genotypes in the dark (D) or blue light (B, 30 μmol m^{-2} s^{-1}). The data are presented as mean ± s.e.m. Half-life ($t_{1/2}$), *P* values (two-tailed Student's *t*-test) and the number of independent experiments (*n*) are shown in graphs. **g**, Hypothetical model depicting the mechanism of CRY-mediated photo-entrainment in plant cells. In blue light, CRY2 (blue nucleus) undergoes LLPS to condense into photobodies, where the CRY2 homotetramer interacts with MTA, MTB and FIP37. The CRY2/writer complex regulates installation of m^6A marks on COGs. Unmodified mRNAs are degraded faster by ribonucleases (Pac-Man) than m6A-modified mRNAs which are translated and imported into the nucleus for the molecular oscillator. ZT, Zeitgeber time.

lengthening in both white and blue light, the *mta* mutant exhibits a relatively stronger long-period phenotype in white light than in blue light (Fig. 4c,d). This seemingly perplexing observation can be explained by the complex redundant and antagonistic functions of phytochromes and CRYs under different light conditions[4,36,37,39]. Importantly, the *cry1cry2* mutant ($P < 0.0001$), but not the *mta* mutant ($P = 0.21$), exhibits a significantly flattened slope of period-shortening in response to increasing blue-light intensity (Fig. 4d) and dramatically reduced robustness of rhythmicity in response to decreasing blue-light intensity (Fig. 4e). These results highlight the photoreceptor function of CRYs and dual function of CRYs regulating RNA methylation (Fig. 1) and transcription[1,4] in the control of photo-entrainment. Consistent with the hypothesis that light-induced LLPS of CRY2 is a mechanism underlying light regulation of mRNA methylation, the abundance of m^6A-modified *CCA1* mRNA decreases significantly in seedlings treated with the LLPS inhibitor 1,6-hexanediol, or is impaired with PPK kinases required to maintain the CRY2 photobody in the liquid phase (Fig. 3h–j) or overexpressing BIC2, an inhibitor of CRY2 photo-oligomerization and photobody formation[18,26] (Extended Data Fig. 4h,i).

Given that m^6A modification generally stabilizes mRNAs in *Arabidopsis*[11], and that CRYs mediate blue-light regulation of m^6A methylation of *CCA1* mRNA (Figs. 1h and 4b), we analysed the

mRNA stability of *CCA1* in response to blue light in both *cry1cry2* and *mta* mutants. In WT seedlings, *CCA1* mRNA exhibited a significantly shortened half-life and faster decay in response to blue light (Fig. 4f), suggesting that blue light stimulates the degradation of *CCA1* mRNA. Importantly, mutations of the *CRY* or *MTA* genes further shortened the half-life of *CCA1* mRNA or accelerated its degradation in light-grown *cry1cry2* and *mta* mutant seedlings (Fig. 4f). In comparison with WT seedlings, the stability of *CCA1* mRNA is not significantly changed in dark-grown *cry1cry2* or *mta* mutants, but is dramatically decreased in light-grown *cry1cry2* or *mta* mutant seedlings with the half-life being reduced by several orders of magnitude in both mutants (Fig. 4f). These results are consistent with the hypothesis that blue-light regulation of the CRY2/MTA complex alters m^{6}A mRNA methylation, mRNA stability and photo-entrainment of the circadian clock in *Arabidopsis*.

Discussion

This study demonstrates that plant CRYs mediate light regulation of mRNA methylation to affect photoresponsive gene expression. We also show that light induces the liquid-phase condensation of CRY2 and co-condensation of the CRY2/writer complex without altering the apparent affinity or nuclear stoichiometry of the interacting proteins. This phenomenon represents the photoresponsive signalling mechanism of a photoreceptor that is different from conventional mechanisms entailing changes in affinity between photoreceptors and their partner proteins[4,40,41]. Liquid-phase photoreceptor condensation resulting from multivalent interactions may alter protein conformation without changing the apparent affinity of the photoreceptors and signalling proteins. Light-induced co-condensation of the CRY2/writer complex in the CRY2 photobody may increase the local concentration and overall catalytic activity of the m^{6}A writer complex at the subnuclear foci of CRY2 photobodies, with or without changing the specific activity of the writer enzymes. CRY2 and CRY2/MTA complex molecules are highly mobile in and out of the CRY2 photobody (Figs. 2l and 3c), but the exact nature of such molecular mobility remains unclear. Interestingly, we found that the mobility of the CRY2 photobody is ~50% that of the random Brownian movement of particles but comparable with that of transcription factors (Supplementary Video 4 and Extended Data Fig. 5d,e). Given the co-transcriptional nature of the m^{6}A RNA methylation process catalysed by METTL3/14-type m^{6}A writers in various model systems[13–15], physical interaction of CRYs with various transcription factors[4] and the physical interaction of MTA and RNA polymerase II[42], it is conceivable that CRY2 and m^{6}A writer molecules co-condensed in the CRY2 photobody may be physically associated with chromatin meshes and transcriptional apparatus. Whether and how CRY2-mediated light regulation of transcription and RNA methylation may be associated spatially and mechanistically remains to be investigated.

Regulation of transcription and protein degradation are the two well-known mechanisms underlying photoreceptor-mediated light control of the circadian clock and other photoresponses in plant development. Results of our study argue for a different mechanistic explanation for the CRY-mediated light regulation of gene expression and the circadian clock (Fig. 4g). According to this model, photo-excited CRY2 undergoes LLPS to recruit and concentrate m^{6}A writer into the CRY2 photobody. The photo-condensed CRY2/writer complex facilitates m^{6}A methylation of mRNA encoding *CCA1* in response to blue light, thus suppressing degradation of the *CCA1* mRNA and period lengthening of the circadian clock. This is consistent with the hypothesis that CRYs mediate light regulation of period length and parametric entrainment of the circadian clock[3,37,43]. However, at least three major issues remain unclear. First, do other photoreceptors also regulate mRNA methylation? For example, phytochromes show complex wavelength dependency and functional interactions with CRYs in mediating photoresponses of the circadian clock in plants[36,37]. It would be interesting to examine possible roles of phytochromes and/or other photoreceptors in the light regulation of m^{6}A mRNA methylation. Second, CRYs affect m^{6}A methylation of mRNAs corresponding to at least ten COGs, but how CRY-dependent light regulation of RNA methylation affects various aspects of the metabolism of mRNAs encoding those COG genes is not clear. It is known that RNA methylation modulates mRNA splicing, nuclear exportation, degradation and translation[13,15,19], and that light regulates mRNA splicing and translation[44–48]. Therefore, one would expect that light-regulated m^{6}A mRNA methylation may modulate activity of the circadian clock by affecting aspects of mRNA metabolism in addition to mRNA degradation. Analyses of the relationship between photoresponsive m^{6}A methylation and various aspects of mRNA metabolism of those COGs would further our understanding how light regulates the circadian clock in plants and other organisms. Finally, CRY is the only key regulator of the circadian clock currently known to be evolutionarily conserved in plants and metazoans, and it appears intriguing that the CRY/writer protein complex is found in both *Arabidopsis* and human cells (Fig. 2). Given the correlated changes in m^{6}A RNA modification, circadian period and metabolism of mRNAs encoding components of the molecular oscillators in evolutionary lineages as remote as *Arabidopsis* (Fig. 4g) and mammals[8–10], it would be interesting to investigate how the CRY/writer complex is involved in regulation of the circadian clock in other plants and non-plant species.

Methods

This research complies with all relevant ethical regulations.

Plant materials and growth conditions. All WT, mutants and transgenic lines used in this study were *Arabidopsis thaliana* Columbia (Col) accessions. *cry1cry2*, *CRY2–GFP/cry1cry2*, *ABI3::MTA/mta*, *pCCA1::LUC*/Col-0 and *pTOC1::LUC*/Col-0 have been described previously[27,38,49,50]. To prepare transgenic lines overexpressing *Flag-MTA–mRFP* or *Flag-GFP–FIP37*, a *pACT2::Flag-MTA–mRFP* or *pACT2::Flag-GFP–FIP37* construct was introduced into the *rdr6-11* allele which suppresses gene silencing[51] or the *Myc-CRY2* transgenic line[26]. To prepare transgenic lines with circadian clock reporter, *pCCA1::LUC* and *pTOC1::LUC* constructs were transformed into *ABI3::MTA/mta* or *cry1cry2* backgrounds. All transgenic lines were generated using the standard floral-dip method[52]. Transgenic T1 populations were screened either on MS–agar media containing 25 mg l^{-1} glufosinate (Cayman Chemical, catalogue no. 16675) or on compound soil watered with BASTA solution. A light-emitting diode was used to generate monochromatic blue light (peak 450 nm; half-bandwidth of 20 nm) and cool white fluorescent tubes were used for white light. The *Arabidopsis* seedlings used in these experiments were grown in either a growth chamber (Conviron, model no. E7/2) or growth room at 21 °C under different light regimes.

Protein expression constructs. All DNA constructs used in this study were prepared by In-Fusion Cloning which allows ligation-independent cloning of polymerase chain reaction (PCR) products into any vector.

To prepare *pACT2::Flag-MTA–mRFP* binary plasmid, DNA fragments of *MTA*, *mRFP* and XmaI/BamHI-digested *pACT2::Flag-GFP* vector (*GFP* coding sequence (CDS) was released) for the In-Fusion reaction were mixed using an In-Fusion HD cloning kit (TaKaRa, catalogue no. 639650). To prepare *pACT2::Flag-GFP–FIP37* binary plasmids, the CDS of *FIP37* was cloned into BamHI-digested *pACT2::Flag-GFP* vector. To generate *35S::Flag-CRY2–YFP*, *35S::Flag-CRY2^{D387A}–YFP*, *35S::CRY2^{C490}–YFP* (CRY2^{C490} indicates 490–612 amino acids of CRY2 protein), *35S::Flag-CRY2^{C510}–YFP* (CRY2^{C510} indicates amino acids 510–612 of CRY2 protein), *35S::Flag-MTA–YFP*, *35S::Flag-MYB–YFP* and *35S::Flag-FIP37–YFP* for transient expressions in protoplasts, the CDS regions of *CRY2*, *CRY2^{D387A}*, *CRY2^{C490}* and *CRY2^{C510}* were PCR-amplified using different plasmids as the templates, and the CDS of *MTA*, *MTB* and *FIP37* were PCR-amplified from *Arabidopsis* cDNA. The 3′-ends of all above DNA fragments were overlapped with the 5′-end of *YFP* CDS. Each DNA fragment with *YFP* CDS were assembled into XmaI/BamHI-digested *35S::Flag-GFP* vector (*GFP* CDS was released) using the In-Fusion method. To prepare *35S::Flag-NLS-CRY2^{N489}–YFP* (CRY2^{N489} indicates amino acids 1–489 of CRY2 protein) and *35S::Flag-NLS-CRY2^{N509}–YFP* (CRY2^{N509} indicates amino acids 1–509 of CRY2 protein), the *Nuclear Localization Signal* (*NLS*) coding sequence was added to the 5′-end of forward primers for cloning *CRY2^{N489}* or *CRY2^{N509}*, the resulting PCR products and *YFP* CDS were assembled into XmaI/BamHI-digested *35S::Flag-GFP* vector by In-Fusion. To prepare *35S::Flag-CRY2–DsRed* and *35S::Flag-MTA–DsRed*,

PCR-amplified *CRY2* or *MTA* CDS mixed with *DsRed* CDS were inserted into XmaI/BamHI-digested *35S::Flag-GFP* vector by In-Fusion. To generate plasmids for BiFC assay, the sequences encoding the N terminus (nYFP; amino acids 1–157) and C terminus (cYFP; amino acids 158–239) of YFP were amplified by PCR, and mixed with *CRY2*, *CRY2*^{D387A}, *MTA*, *MTB* or *FIP37* CDS for in-fusion into XmaI/BamHI-digested *35S::Flag-GFP* vector to produce *35S::CRY2–nYFP*, *35S::CRY2*^{D387A}*-nYFP*, *35S::MTA–cYFP*, *35S::MTB–cYFP* and *35S::FIP37–cYFP*.

To generate mammalian cell expression plasmids *pQCMV-Flag-CRY2*, *pQCMV-Flag-CRY2*^{N489} and *pQCMV-Flag-CRY2*^{C490} for co-immunoprecipitation assays, PCR-amplified *CRY2*, *CRY2*^{N489} and *CRY2*^{C490} CDS were added by In-Fusion to SpeI/KpnI-digested *pQCMV-Flag-GFP* (*GFP* CDS was released). To prepare *pCMV-Myc-MTA*, *pCMV-Myc-MTA*^{N350} (MTA^{N350} indicates amino acids 1–350 of MTA protein), *pCMV-Myc-MTA*^{C351} (MTA^{C351} indicates amino acids 351–685 of MTA protein), *pCMV-Myc-MTB* and *pCMV-Myc-FIP37*, *pCMV-Myc-METTL3* for co-immunoprecipitation assays, the CDS of *MTA*, *MTA*^{N350}, *MTA*^{C351}, *MTB*, *FIP37* and human *METTL3* were amplified by PCR and assembled into BamHI-digested *pCMV-Myc* vector by In-Fusion. To create *pQCMV-Flag-CRY2–YFP*, *pQCMV-Flag-CRY2*^{N489}*–YFP*, *pQCMV-Flag-CRY2*^{N509}*–YFP*, *pQCMV-Flag-CRY2*^{C490}*–YFP* and *pQCMV-Flag-CRY2*^{C510}*–YFP* for microscopy, the PCR products of CRY2, *CRY2*^{N489}, *CRY2*^{N509}, *CRY2*^{C490} or *CRY2*^{C510} CDS were mixed with YFP CDS for in-fusion into SpeI/KpnI-digested *pQCMV-Flag-GFP* vector. To prepare *pQCMV-GFP–hCRY2* for teh co-immunoprecipitation assay, PCR-amplified human *CRY2* (*hCRY2*) CDS was cloned into SpeI-digested *pQCMV-EGFP* vector by In-Fusion. All cloned sequences in plasmids were verified by Sanger sequencing.

Protein expression in HEK293T cells. HEK293T cells were maintained in DMEM supplemented with 10% (v/v) fetal bovine serum, 100 IU penicillin and 100 mg l^{-1} streptomycin, in humidified 5% (v/v) CO_2 air, at 37 °C (ref. [26]). HEK293T cells were seeded in 10 cm plates at a density of ~2.4 × 10^6 cells/plate and transfected using a calcium phosphate precipitation protocol. For each transfection, plasmid DNA (10–15 μg) was mixed with 60 μl of 2.5 M $CaCl_2$ and double-distilled H_2O to a total volume of 600 μl, then 600 μl of 2× HeBS (250 mM NaCl, 10 mM KCl, 1.5 mM Na_2HPO_4, 12 mM dextrose and 50 mM HEPES pH 7.5, with the pH of the final solution adjusted to 7.05) was added slowly to the mixture while vortexing. The media was aspirated from the culture plate and the transfection mixture added slowly to the plate without disturbing the cells. Six millilitres of media with 25 μM chloroquine was added to each plate. After incubation for 16–20 h, the culture media was replaced with fresh media without chloroquine. Cells were harvested 36–48 h after transfection.

Protein expression in *Arabidopsis* mesophyll protoplasts. Protoplasts were isolated from well-expanded leaves of 3-week-old long-day-grown plants[53]. Leaves were incubated in the enzyme solution (20 mM MES pH 5.7, 1.2% w/v cellulase R10, 0.4% w/v macerozyme R10, 0.4 M mannitol, 20 mM KCl and 10 mM $CaCl_2$) in the dark at room temperature for 2–4 h. Protoplasts in the solution were filtered through one layer of miracloth (Millipore Sigma, catalogue no. 475855-1R) and pelleted by centrifugation at 100*g* for 2 min at 4 °C. Protoplasts were resuspended and washed twice with ice-cold W5 buffer (2 mM MES pH 5.7, 154 mM NaCl, 125 mM $CaCl_2$, 5 mM KCl), then kept in W5 buffer on ice for 30 min. The mixture was centrifuged at 100 × *g* to remove the W5 buffer and the protoplasts resuspended in MMg buffer (4 mM MES pH 5.7, 0.4 M mannitol, 15 mM $MgCl_2$) to a density of ~10^6 protoplasts ml^{-1}. For each transformation, 30 μl of plasmids (~1 μg plasmids μl^{-1}) was mixed with 200 μl of protoplasts and 230 μl pf polyethylene glycol (PEG) solution (40% w/v PEG4000, 0.2 M mannitol, 100 mM $CaCl_2$), and incubated at room temperature for 15 min. After washing, transfected protoplasts were resuspended in 1 ml of W5 buffer and incubated in the dark at room temperature overnight before examination of protein expression.

Co-immunoprecipitation assays. For co-immunoprecipitation using transfected HEK293T cells, the cells were lysed in Brij buffer (1% Brij-35, 50 mM Tris–HCl pH 8.0, 150 mM NaCl, 1 mM PMSF and 1× protease inhibitor cocktail). After centrifugation at 13,000*g* for 10 min at 4 °C, the supernatant was either saved as the 'input' or mixed with 20 μl of FLAG M2 beads (Sigma, catalogue no. F2426) and incubated at 4 °C for 2 h with gentle rotation. Beads were pelleted and washed five times with Brij buffer (without protease inhibitors). Proteins were eluted from beads using 25 μl of 3× Flag peptide solution (150 ng μl^{-1} in Brij buffer with 1 mM PMSF and 1× protease inhibitor cocktail). Both 'input' and eluted proteins were mixed with 5× SDS sample buffer (250 mM Tris–HCl pH 6.8, 10% SDS, 0.5 M dithiothreitol, 0.5% bromophenol blue and 50% glycerol) and denatured at 100 °C for 5 min.

For co-immunoprecipitation using *Arabidopsis*, plants were grown in long days for two weeks, and kept in the dark for 24 h before harvest. Rosette leaves from dark-adapted plants or plants illuminated with blue light (30 μmol m^{-2} s^{-1}) were collected. The tissues were ground in liquid N_2 and homogenized in an equal volume of immunoprecipitation buffer (IP buffer; 50 mM Tris–HCl pH 7.4, 150 mM NaCl,1% Triton X-100, 1 mM PMSF, 2 mM NaF and 1× protease inhibitor cocktail). The tissue lysate was filtered through one layer of miracloth and centrifuged at 13,000*g* for 10 min at 4 °C. The supernatant was either saved as the 'input' or mixed with 20 μl of FLAG M2 beads and incubated at 4 °C for 2 h with gentle rotation. Beads were pelleted and washed four times with IP buffer (without protease inhibitors). The proteins were eluted from the beads with 2× SDS sample buffer by heating at 100 °C for 5 min.

Protein samples were analysed by 10% SDS–PAGE and immunoblots. The primary antibodies used in this study are anti-CRY2 (1:3,000)[39], anti-FLAG (1:3,000; Sigma, catalogue no. F3165) and anti-Myc (1:3,000; Millipore, catalogue no. 05-724).

Image acquisition and analysis. All microscopic images were taken by a Zeiss LSM 780 confocal microscope with a Plan-Apochromat ×63/1.40 oil DIC M27 objective controlled by ZEN software. For time-lapse imaging of CRY2 photobodies, a chamber (1 × 1 cm^2) was created on the slide using SecureSeal adhesive sheets (120 μm thick; Grace Bio-Labs, catalogue no. 620001). The slide was placed on the microscope and a 488 nm laser used to scan the sample for 60 s to induce CRY2 photobodies. GFP signals were then detected at 493–598 nm using an excitation wavelength of 488 nm. To observe the inhibition of CRY2–YFP photobody formation, protoplasts were incubated in W5 buffer with 1,6-hexanediol (10%) for 5 min in the dark then illuminated with a 488 nm laser. To observe DsRed or YFP fusion proteins (including BiFC signals) in a time-series over the blue laser illumination, protoplasts or HEK293T cells in the slide chamber were rapidly screened under green fluorescence to locate cells positive for DsRed or YFP signals. YFP was then excited with a 514 nm laser and detected at 520–620 nm; DsRed was excited with a 561 nm laser and detected at 566–629 nm. Images were acquired in a time-series in which the first image was taken with the 488 nm laser off (T0) and the remainder were taken with the 488 nm laser on (1% laser power). Image analysis was performed using FIJI/ImageJ[54].

Fluorescence recovery after photobleaching assay. In vivo FRAP assays of CRY2 photobodies or photobody-like structures were performed as described previously[55]. For FRAP of CRY2–GFP photobodies in transgenic plants, 3-day-old etiolated *35S::CRY2–GFP/cry1cry2* seedlings were exposed to blue light from a 488 nm laser (1% laser power) for 1 min before photobleaching. For FRAP of CRY2–YFP photobodies in protoplasts, the dark-incubated protoplasts were illuminated by blue light from a 488 nm laser (1% laser power) for 30 s, a single photobody of CRY2–YFP or CRY2/MTA BiFC complex was then used for each FRAP assay. The selected CRY2 photobody was photobleached using a 488 nm laser (100 iterations; 90% of laser power) for CRY2–GFP or a 514 nm laser (100 iterations; 90% of laser power) for CRY2–YFP or CRY2/MTA BiFC. Time-lapse images of fluorescence recovery were taken every 1 s for at least 1 min. The fluorescence intensities of both photobleached and other regions in the images were measured with FIJI/ImageJ to meet the requirement for further analysis using easyFRAP software[56]. Full-scale normalization was performed with each fluorescence recovery curve. The normalized data were then fitted using a double exponential model: $I(t) = I_0 - \alpha e^{-\beta t} - \gamma e^{-\delta t}$ (where I_0 is the summit or plateau of the curve; α, β, γ and δ are algorithm parameters defined by the EasyFRAP software for curve fitting[56]. The maximum value of fitting iterations was set to 1,000, while the starting values of the parameters were set at $I_0 = 0.85$, $\alpha = 0.5$, $\beta = 0.563$, $\gamma = 0.316$ and $\delta = 0.36$. For the full-scale normalized curve with the maximum analytic time, the mobile fraction (mf) equals I_0 (ref. [56]). Mobility is defined as the rate of fluorescence recovery after photobleaching.

CRY2 photobodies tracking and analysis. To analyse the motion of CRY2 photobodies in *CRY2–GFP* transgenic plants, seedlings were illuminated using a 488 nm laser (1% laser power) for 1 min, then time-lapse images were taken every 3 s for 10 min. To track CRY2 photobodies, each series of time-lapse images was first aligned using the Template Matching plugin[57] in FIJI imageJ and then stacked. CRY2 photobody tracking and trajectory analysis of image stacks were performed using SpatTrack[58]. Briefly, images denoised through the boxcar filter were used to track photobodies. Then mean square displacement (MSD) of the generated trajectory was fitted to an anomalous diffusion model: $\mathrm{MSD}(t) = 4D_\alpha t^\alpha$ (where t is the time, α *is* the anomalous exponent, which depends on the type of anomalous diffusion ($0 < \alpha < 1$ for anomalous subdiffusion and $1 < \alpha < 2$ for anomalous superdiffusion) and D is the diffusion constant).

Other image quantification analyses. To measure the circularity and aspect ratio of CRY2 photobodies or photobody-like structures, images were first converted to 8-bit binary images then 'Analyse particles' was performed to obtain 'shape descriptors'. Circularity is defined as 4π × (area/(square of perimeter)), and the aspect ratio is calculated as major axis/minor axis.

The partition coefficient is calculated as the ratio of the mean fluorescence intensity between the condensed and dispersed phases[59]. Specifically, the mean fluorescence intensity was quantified either inside the photobody (I_{inside}) or in the immediately adjacent region outside the photobody (I_{outside}); the partition coefficient is then calculated by taking the ratio of I_{inside} to I_{outside}.

In vivo bioluminescence assay. WT, *cry1cry2* and *ABI3::MTA/mta* seedlings harbouring a *pCCA1::LUC* or *pTOC1::LUC* reporter were entrained in a photoperiod of 12 h white light (~90 μmol m^{-2} s^{-1}) and 12 h dark at 21 °C for

6 days and transferred to a 96-well plate (a seedling/well) containing 200 µl of MS–agar media per well; 30 µl of 2.5 mM luciferin was then added to each well. The 96-well plate was kept under continuous white light (~90 µmol m^{-2} s^{-1}). Bioluminescence was measured every 1 h over 5–7 days using a Centro LB960 Microplate Luminometer (Berthold Technologies) with Microwin 2000 software.

For fluence response curves, *pCCA1::LUC/cry1cry2 or ABI3::MTA/mta* lines were prepared by crossing *cry1cry2* or *ABI3::MTA/mta* mutants with *pCCA1::LUC*/WT. Seedlings of *pCCA1::LUC* reporter lines were entrained in a photoperiod of 12 h white light (~90 µmol m^{-2} s^{-1}) and 12 h dark at 21 °C for 6 days, before being released into continuous blue light with various fluence rates. On the first day in blue light, seedlings were transferred to a 96-well plate. The 96-well plates were loaded manually into a Modulus microplate reader (Promega) every 3 h for 6 days to measure the bioluminescence.

The circadian period analysis, bioluminescence normalization and rhythmicity test were performed using BioDare2 (https://www.biodare2.ed.ac.uk)[60,61]. Specifically, the period was estimated using the fast Fourier transform non-linear least squares method and the relative amplitude error was calculated to evaluate the robustness of oscillation of individual samples. Relative amplitude error values of 0 and 1 indicate perfect oscillation and arrhythmicity, respectively. Rhythmicity analysis was performed using the BD2 eJTK method[60,62], through which the Kendall τ rank correlation coefficient (τ coefficient) between the data and a reference function (with different phases) was calculated. Perfectly correlated data scores have $\tau = 1$ and uncorrelated data scores have $\tau = 0$.

RNA stability analysis. WT, *cry1cry2* and *ABI3::MTA/mta* seedlings were grown on MS–agar plates in the dark or in blue light (30 µmol m^{-2} s^{-1}) for 6 days, then treated with cordycepin (transcription inhibitor) as described[63,64]. Briefly, seedlings were incubated in vacuum buffer (15 mM sucrose, 1 mM KCl, 1 mM PIPES pH 6.25 and 1 mM sodium citrate) for 15 min before the vacuum buffer was replaced with fresh buffer containing 1 mM cordycepin (AdooQ Bioscience, catalogue no. NC1769697). Seedlings were vacuumed for 2 min and collected as T0 samples. The remaining seedlings were vacuumed again for 2 min, and collected at 7.5, 15, 30, 60 and 120 min following the first vacuum release.

Total RNA was prepared using a Monarch Total RNA Miniprep Kit (NEB, catalogue no. T2010S). cDNA was synthesized from 1 µg of total RNA with oligo-dT primers using SuperScript IV First-Strand Synthesis System (Invitrogen, catalogue no. 18091050). Quantitative PCR (qPCR) was performed with SYBR Green qPCR SuperMix-UDG (Invitrogen, catalogue no. 11733-038) on a Mx3005P real-time PCR system (Stratagene). The qPCR results for the tested genes were first normalized to the internal control gene *LTPG1* (AT1G27950, which is non-photoresponsive and lacks m^6A deposition on RNA), then renormalized to T0 for each time-series using the ΔΔCt method[65]. The obtained mRNA decay curve was fitted with a one-phase exponential decay model using GraphPad Prism 8 to estimate the half-life ($t_{1/2}$)[66].

RNA-seq and data analysis. Total RNA isolated from WT and *cry1cry2* seedlings grown in the dark or in blue light (30 µmol m^{-2} s^{-1}) for 6 days was used to prepare RNA-seq libraries with TruSeq RNA library prep kit (Illumina). The libraries from three biological repeats for each sample were sequenced on the Illumina HiSeq 2500 sequencing systems in pair-end mode with 125 bp per read. After sequencing, the pair-end reads were aligned to the *Arabidopsis* TAIR10 genome using Tophat-2.0.11 with an anchor length longer than eight nucleotides for spliced alignments[67]. Only uniquely mapped reads were retained for subsequent analysis. The expression levels for gene models from TAIR10 were measured and normalized as fragments per kilobase of transcript per million mapped reads[68,69].

m^6A-seq (MeRIP-seq) and data analysis. WT and *cry1cry2* seedlings grown in the dark or in blue light (30 µmol m^{-2} s^{-1}) for 6 days were used for m^6A-seq[16]. Total RNA was isolated using HiPure Universal RNA Maxi kit (Magen, catalogue no. R4132-02). Approximately 2 mg of RNA for each sample was dissolved in 1.8 ml of RNase-free H_2O. For each fragmentation reaction (60 µl), 54 µl of RNA was mixed with 6 µl of 10× fragmentation buffer (100 mM Tris–HCl pH 7.0 and 100 mM $ZnCl_2$), and incubated at 94 °C for 5 min. Then 6 µl of 0.5 M EDTA was immediately added to each reaction. For RNA precipitation, every eight fragmentation reactions (~480 µl) from the same sample were pooled and mixed with 48 µl of 3 M sodium acetate (pH 5.2), 12 µl of glycogen (5 mg ml^{-1}) and 1.2 ml of 100% ethanol. The RNA at was incubated at −80 °C overnight then centrifuged at 13,000*g* for 30 min at 4 °C to give a pellet. The RNA pellet was washed with 1 ml of 75% ethanol, air-dried and dissolved in RNase-free H_2O. Fifteen micrograms of fragmented RNA was saved as the 'input'. For each immunoprecipitation reaction, ~2 mg fragmented RNA was mixed with 10 µl of RNasin Plus (40 U $µl^{-1}$; Promega, catalogue no. N2611), 20 µl of m^6A-specific antibody (0.5 mg ml^{-1}; Synaptic Systems, catalogue no. 202003) and 200 µl of 5× IP buffer (50 mM Tris–HCl pH 7.4, 750 mM NaCl and 0.5% v/v Igepal CA-630), and RNase-free H_2O was added to give a final volume of 1 ml. The immunoprecipitation reaction was incubated at 4 °C for 2 h with gentle rotation. Meanwhile, 100 µl of protein A/G magnetic beads (Thermo Scientific, catalogue no. 88803) were washed twice with 1× IP buffer and the beads resuspended with 1 ml of 1× IP with bovine serum albumin (0.5 mg ml^{-1}) and incubated at 4 °C for 2 h with rotation. The supernatant was removed from the beads which were then mixed with 1 ml of IP buffer and incubated at 4 °C for 2 h with rotation. Beads were then washed four times with 1× IP buffer and the RNA eluted with 100 µl of elution buffer (10 mM Tris–HCl pH 7.4, 150 mM NaCl, 0.1% Igepal CA0630, 2 µl of RNasin Plus and 6.7 mM m^6A) at 4 °C for 1 h with vigorous shaking. The elution was repeated once and the two elutes combined (~ 200 µl in total). Then 20 µl of 3 M sodium acetate (pH 5.2) and 500 µl of 100% ethanol were added to the elutes and the mixtures kept at −80 °C overnight. The RNA was pelleted and washed once with 75% ethanol, air-dried and dissolved in RNase-free H_2O. Between 100 and 200 ng of 'input' or 'immunoprecipitation' RNA was used for sequencing library preparations according to instructions given in the TruSeq RNA library prep kit (Illumina). The libraries from three biological repeats for each sample were sequenced on Illumina Novaseq6000 instruments in pair-end mode with 150 bp per reads.

After sequencing, the fastx_clipper script from FASTX-toolkit (http://hannonlab.cshl.edu/fastx_toolkit) was used for adaptor sequence trimming of FASTQ files from input and immunoprecipitation samples using following parameters: -l 20 -d 0 -n -v -M 6. The above clean reads were then aligned to the *Arabidopsis* reference genome (TAIR10) using TopHat v.2.0.11 with the following parameters: -a 8 -m 0, which required the minimum anchor length; the maximum number of mismatches for junction reads was 8 and 0, respectively. The uniquely mapped reads for each peak from the immunoprecipitation and input samples were calculated. Differences between the immunoprecipitation and input samples were evaluated with sliding windows of 25 nucleotides to perform Fisher's exact test and multiple testing using Benjamini–Hochberg[70]. Significant m^6A regions were indicated if the false discovery rate was <0.01. The number of reads covering each base were calculated using SAMtools[71] from the alignment results in BAM format. Normalized m^6A signals for each significant m^6A region (transcripts per million) were calculated using the following formula: number of reads covering m^6A region × 10^6/total reads. In this study, we collected overlapping CCG from previously published circadian gene expression data sets[72–75].

Statistics and reproducibility. Statistical analysis by a two-tailed *t*-test was performed using Microsoft Excel. Model fitting to curves was performed using GraphPad Prism v.8. No statistical method was used to predetermine sample size, which was estimated based on previous established protocols in the field. All experiments were repeated independently at least twice and showed similar results.

Reporting Summary. Further information on research design is available in the Nature Research Reporting Summary linked to this article.

Data availability

All data supporting the findings of this study are available in the main text or the supplementary table. Biological materials used in this study are available from C.L. on reasonable request. The m^6A-seq and RNA-seq data reported in this study have been deposited in the NCBI Gene Expression Omnibus under accession number GSE152466 which is fully available. The RNA-seq data for WT and *cry1cry2* sample in the dark condition have been reported previously (GSE80350)[26]. Source data are provided with this paper.

Received: 9 March 2021; Accepted: 3 August 2021;
Published online: 14 October 2021

References

1. Sanchez, S. E., Rugnone, M. L. & Kay, S. A. Light perception: a matter of time. *Mol. Plant* **13**, 363–385 (2020).
2. Patke, A., Young, M. W. & Axelrod, S. Molecular mechanisms and physiological importance of circadian rhythms. *Nat. Rev. Mol. Cell Biol.* **21**, 67–84 (2020).
3. Webb, A. A. R., Seki, M., Satake, A. & Caldana, C. Continuous dynamic adjustment of the plant circadian oscillator. *Nat. Commun.* **10**, 550 (2019).
4. Wang, Q. & Lin, C. Mechanisms of cryptochrome-mediated photoresponses in plants. *Annu. Rev. Plant Biol.* **71**, 103–129 (2020).
5. Cashmore, A. R. Cryptochromes: enabling plants and animals to determine circadian time. *Cell* **114**, 537–543 (2003).
6. Sancar, A. Cryptochrome: the second photoactive pigment in the eye and its role in circadian photoreception. *Annu. Rev. Biochem.* **69**, 31–67 (2000).
7. Bailey-Serres, J., Zhai, J. & Seki, M. The dynamic kaleidoscope of RNA biology in plants. *Plant Physiol.* **182**, 1–9 (2020).
8. Parker, M. T. et al. Nanopore direct RNA sequencing maps the complexity of *Arabidopsis* mRNA processing and m(6)A modification. *eLife*; https://doi.org/10.7554/eLife.49658 (2020).
9. Wang, C. Y., Yeh, J. K., Shie, S. S., Hsieh, I. C. & Wen, M. S. Circadian rhythm of RNA N6-methyladenosine and the role of cryptochrome. *Biochem. Biophys. Res. Commun.* **465**, 88–94 (2015).
10. Fustin, J. M. et al. RNA-methylation-dependent RNA processing controls the speed of the circadian clock. *Cell* **155**, 793–806 (2013).

11. Anderson, S. J. et al. N^6-Methyladenosine inhibits local ribonucleolytic cleavage to stabilize mRNAs in *Arabidopsis*. *Cell Rep.* **25**, 1146–1157 e1143 (2018).
12. Wang, X. et al. N6-methyladenosine-dependent regulation of messenger RNA stability. *Nature* **505**, 117–120 (2014).
13. Zaccara, S., Ries, R. J. & Jaffrey, S. R. Reading, writing and erasing mRNA methylation. *Nat. Rev. Mol. Cell Biol.* **20**, 608–624 (2019).
14. Shen, L., Liang, Z., Wong, C. E. & Yu, H. Messenger RNA modifications in plants. *Trends Plant Sci.* **24**, 328–341 (2019).
15. Zhao, B. S., Roundtree, I. A. & He, C. Post-transcriptional gene regulation by mRNA modifications. *Nat. Rev. Mol. Cell Biol.* **18**, 31–42 (2017).
16. Dominissini, D., Moshitch-Moshkovitz, S., Salmon-Divon, M., Amariglio, N. & Rechavi, G. Transcriptome-wide mapping of N(6)-methyladenosine by m(6)A-seq based on immunocapturing and massively parallel sequencing. *Nat. Protoc.* **8**, 176–189 (2013).
17. Wang, Z. Y. & Tobin, E. M. Constitutive expression of the *CIRCADIAN CLOCK ASSOCIATED 1* (*CCA1*) gene disrupts circadian rhythms and suppresses its own expression. *Cell* **93**, 1207–1217 (1998).
18. Liu, Q. et al. Molecular basis for blue light-dependent phosphorylation of *Arabidopsis* cryptochrome 2. *Nat. Commun.* **8**, 15234 (2017).
19. Arribas-Hernandez, L. & Brodersen, P. Occurrence and functions of m(6)A and other covalent modifications in plant mRNA. *Plant Physiol.* **182**, 79–96 (2020).
20. Ruzicka, K. et al. Identification of factors required for m^{6}A mRNA methylation in *Arabidopsis* reveals a role for the conserved E3 ubiquitin ligase HAKAI. *New Phytol.* **215**, 157–172 (2017).
21. Zhong, S. et al. MTA is an *Arabidopsis* messenger RNA adenosine methylase and interacts with a homolog of a sex-specific splicing factor. *Plant Cell* **20**, 1278–1288 (2008).
22. Chen, Y. et al. Regulation of *Arabidopsis* photoreceptor CRY2 by two distinct E3 ubiquitin ligases. *Nat. Commun.* **12**, 2155 (2021).
23. Yu, X. et al. *Arabidopsis* cryptochrome 2 completes its posttranslational life cycle in the nucleus. *Plant Cell* **19**, 3146–3156 (2007).
24. Liu, Q. et al. Photooligomerization determines photosensitivity and photoreactivity of plant cryptochromes. *Mol. Plant* **13**, 398–413 (2020).
25. Liu, H. et al. Photoexcited CRY2 interacts with CIB1 to regulate transcription and floral initiation in *Arabidopsis*. *Science* **322**, 1535–1539 (2008).
26. Wang, Q. et al. Photoactivation and inactivation of *Arabidopsis* cryptochrome 2. *Science* **354**, 343–347 (2016).
27. Yu, X. et al. Formation of nuclear bodies of *Arabidopsis* CRY2 in response to blue light is associated with its blue light-dependent degradation. *Plant Cell* **21**, 118–130 (2009).
28. Mas, P., Devlin, P. F., Panda, S. & Kay, S. A. Functional interaction of phytochrome B and cryptochrome 2. *Nature* **408**, 207–211 (2000).
29. Sabari, B. R. et al. Coactivator condensation at super-enhancers links phase separation and gene control. *Science* https://doi.org/10.1126/science.aar3958 (2018).
30. Bracha, D. et al. Mapping local and global liquid phase behavior in living cells using photo-oligomerizable seeds. *Cell* **175**, 1467–1480 e1413 (2018).
31. Shin, Y. et al. Spatiotemporal control of intracellular phase transitions using light-activated optodroplets. *Cell* **168**, 159–171 e114 (2017).
32. Dignon, G. L., Best, R. B. & Mittal, J. Biomolecular phase separation: from molecular driving forces to macroscopic properties. *Annu. Rev. Phys. Chem.* **71**, 53–75 (2020).
33. Alberti, S., Gladfelter, A. & Mittag, T. Considerations and challenges in studying liquid–liquid phase separation and biomolecular condensates. *Cell* **176**, 419–434 (2019).
34. Wang, Q. et al. The blue light-dependent phosphorylation of the CCE domain determines the photosensitivity of *Arabidopsis* CRY2. *Mol. Plant* **8**, 631–643 (2015).
35. Shalitin, D. et al. Regulation of *Arabidopsis* cryptochrome 2 by blue-light-dependent phosphorylation. *Nature* **417**, 763–767 (2002).
36. Devlin, P. F. & Kay, S. A. Cryptochromes are required for phytochrome signaling to the circadian clock but not for rhythmicity. *Plant Cell* **12**, 2499–2510 (2000).
37. Somers, D. E., Devlin, P. F. & Kay, S. A. Phytochromes and cryptochromes in the entrainment of the *Arabidopsis* circadian clock. *Science* **282**, 1488–1490 (1998).
38. Bodi, Z. et al. Adenosine methylation in *Arabidopsis* mRNA is associated with the 3′ end and reduced levels cause developmental defects. *Front. Plant Sci.* **3**, 48 (2012).
39. Guo, H., Yang, H., Mockler, T. C. & Lin, C. Regulation of flowering time by *Arabidopsis* photoreceptors. *Science* **279**, 1360–1363 (1998).
40. Legris, M., Ince, Y. C. & Fankhauser, C. Molecular mechanisms underlying phytochrome-controlled morphogenesis in plants. *Nat. Commun.* **10**, 5219 (2019).
41. Leivar, P. & Quail, P. H. PIFs: pivotal components in a cellular signaling hub. *Trends Plant Sci.* **16**, 19–28 (2011).
42. Bhat, S. S. et al. mRNA adenosine methylase (MTA) deposits m(6)A on pri-miRNAs to modulate miRNA biogenesis in *Arabidopsis thaliana*. *Proc. Natl Acad. Sci. USA* **117**, 21785–21795 (2020).
43. Aschoff, J. Exogenous and endogenous components in circadian rhythms. *Cold Spring Harb. Symp. Quant. Biol.* **25**, 11–28 (1960).
44. Jang, G. J., Yang, J. Y., Hsieh, H. L. & Wu, S. H. Processing bodies control the selective translation for optimal development of *Arabidopsis* young seedlings. *Proc. Natl Acad. Sci. USA* **116**, 6451–6456 (2019).
45. Godoy Herz, M. A. et al. Light regulates plant alternative splicing through the control of transcriptional elongation. *Mol. Cell* **73**, 1066–1074 e1063 (2019).
46. Wu, S. H. Gene expression regulation in photomorphogenesis from the perspective of the central dogma. *Annu. Rev. Plant Biol.* **65**, 311–333 (2014).
47. Paik, I., Yang, S. & Choi, G. Phytochrome regulates translation of mRNA in the cytosol. *Proc. Natl Acad. Sci. USA* **109**, 1335–1340 (2012).
48. Juntawong, P. & Bailey-Serres, J. Dynamic light regulation of translation status in *Arabidopsis thaliana*. *Front. Plant Sci.* **3**, 66 (2012).
49. Wang, X. et al. SKIP is a component of the spliceosome linking alternative splicing and the circadian clock in *Arabidopsis*. *Plant Cell* **24**, 3278–3295 (2012).
50. Mockler, T. C., Guo, H., Yang, H., Duong, H. & Lin, C. Antagonistic actions of *Arabidopsis* cryptochromes and phytochrome B in the regulation of floral induction. *Development* **126**, 2073–2082 (1999).
51. Harmoko, R. et al. RNA-dependent RNA polymerase 6 is required for efficient hpRNA-induced gene silencing in plants. *Mol. Cells* **35**, 202–209 (2013).
52. Clough, S. J. Floral dip: agrobacterium-mediated germ line transformation. *Methods Mol. Biol.* **286**, 91–102 (2005).
53. Wu, F. H. et al. Tape-*Arabidopsis* Sandwich – a simpler *Arabidopsis* protoplast isolation method. *Plant Methods* **5**, 16 (2009).
54. Schindelin, J. et al. Fiji: an open-source platform for biological-image analysis. *Nat. Methods* **9**, 676–682 (2012).
55. Fang, X. et al. *Arabidopsis* FLL2 promotes liquid–liquid phase separation of polyadenylation complexes. *Nature* **569**, 265–269 (2019).
56. Rapsomaniki, M. A. et al. easyFRAP: an interactive, easy-to-use tool for qualitative and quantitative analysis of FRAP data. *Bioinformatics* **28**, 1800–1801 (2012).
57. Tseng, Q. et al. A new micropatterning method of soft substrates reveals that different tumorigenic signals can promote or reduce cell contraction levels. *Lab Chip* **11**, 2231–2240 (2011).
58. Lund, F. W. et al. SpatTrack: an imaging toolbox for analysis of vesicle motility and distribution in living cells. *Traffic* **15**, 1406–1429 (2014).
59. Ries, R. J. et al. m(6)A enhances the phase separation potential of mRNA. *Nature* **571**, 424–428 (2019).
60. Zielinski, T., Moore, A. M., Troup, E., Halliday, K. J. & Millar, A. J. Strengths and limitations of period estimation methods for circadian data. *PLoS ONE* **9**, e96462 (2014).
61. Moore, A., Zielinski, T. & Millar, A. J. in *Plant Circadian Networks: Methods and Protocols* (ed. Staiger, D.) 13–44 (Springer, 2014).
62. Hutchison, A. L. et al. Improved statistical methods enable greater sensitivity in rhythm detection for genome-wide data. *PLoS Comput. Biol.* **11**, e1004094 (2015).
63. Chantarachot, T. et al. DHH1/DDX6-like RNA helicases maintain ephemeral half-lives of stress-response mRNAs. *Nat. Plants* **6**, 675–685 (2020).
64. Sorenson, R. S., Deshotel, M. J., Johnson, K., Adler, F. R. & Sieburth, L. E. *Arabidopsis* mRNA decay landscape arises from specialized RNA decay substrates, decapping-mediated feedback, and redundancy. *Proc. Natl Acad. Sci. USA* **115**, E1485–E1494 (2018).
65. Pfaffl, M. W. A new mathematical model for relative quantification in real-time RT–PCR. *Nucleic Acids Res.* **29**, e45 (2001).
66. Trcek, T., Larson, D. R., Moldon, A., Query, C. C. & Singer, R. H. Single-molecule mRNA decay measurements reveal promoter-regulated mRNA stability in yeast. *Cell* **147**, 1484–1497 (2011).
67. Kim, D. et al. TopHat2: accurate alignment of transcriptomes in the presence of insertions, deletions and gene fusions. *Genome Biol.* **14**, R36 (2013).
68. Mortazavi, A., Williams, B. A., McCue, K., Schaeffer, L. & Wold, B. Mapping and quantifying mammalian transcriptomes by RNA-Seq. *Nat. Methods* **5**, 621–628 (2008).
69. Trapnell, C. et al. Differential gene and transcript expression analysis of RNA-seq experiments with TopHat and Cufflinks. *Nat. Protoc.* **7**, 562–578 (2012).
70. Luo, G. Z. et al. Unique features of the m6A methylome in *Arabidopsis thaliana*. *Nat. Commun.* **5**, 5630 (2014).
71. Li, H. et al. The Sequence Alignment/Map format and SAMtools. *Bioinformatics* **25**, 2078–2079 (2009).
72. Yang, Y., Li, Y., Sancar, A. & Oztas, O. The circadian clock shapes the *Arabidopsis* transcriptome by regulating alternative splicing and alternative polyadenylation. *J. Biol. Chem.* **295**, 7608–7619 (2020).
73. Romanowski, A., Schlaen, R. G., Perez-Santangelo, S., Mancini, E. & Yanovsky, M. J. Global transcriptome analysis reveals circadian control of splicing events in *Arabidopsis thaliana*. *Plant J.* **103**, 889–902 (2020).

74. Li, S. et al. CGDB: a database of circadian genes in eukaryotes. *Nucleic Acids Res.* **45**, D397–D403 (2017).
75. Covington, M. F., Maloof, J. N., Straume, M., Kay, S. A. & Harmer, S. L. Global transcriptome analysis reveals circadian regulation of key pathways in plant growth and development. *Genome Biol.* **9**, R130 (2008).

Acknowledgements

We thank J. Bailey-Serres for research discussions and manuscript editing, R. G. Fray for providing the *ABI3::MTA/mta* line, R. McClung and X. Xu for providing *pCCA1::LUC* and *pTOC1::LUC* reporter constructs and reporter lines, the UCLA-FAFU Joint Research Center on Plant Proteomics and the UCLA-MCDB/BSCRC Microscopy Core for institutional support. Works in the authors' laboratories are supported in part by the National Natural Science Foundation of China (31970265 to Q.W.), Natural Science Foundation of Fujian Province (2019J06014 to Q.W.), the National Institutes of Health (R01GM056265 to C.L.) and UCLA Sol Leshin Programme (to C.L.).

Author contributions

C.L. and X.W. designed the study and wrote the paper. L.G. performed bioinformatics analyses. X.W., B.C., Y.C., M.M., M.Z., E.N. and Q.W. performed the experiments and analysed the data. Q.W. contributed materials/analysis tools.

Competing interests

The authors declare potential competing interests.

Additional information

Extended data are available for this paper at https://doi.org/10.1038/s41477-021-01002-z.

Supplementary information The online version contains supplementary material available at https://doi.org/10.1038/s41477-021-01002-z.

Correspondence and requests for materials should be addressed to Qin Wang or Chentao Lin.

Peer review information *Nature Plants* thanks Peter Quail and the other, anonymous, reviewer(s) for their contribution to the peer review of this work.

Reprints and permissions information is available at www.nature.com/reprints.

Publisher's note Springer Nature remains neutral with regard to jurisdictional claims in published maps and institutional affiliations.

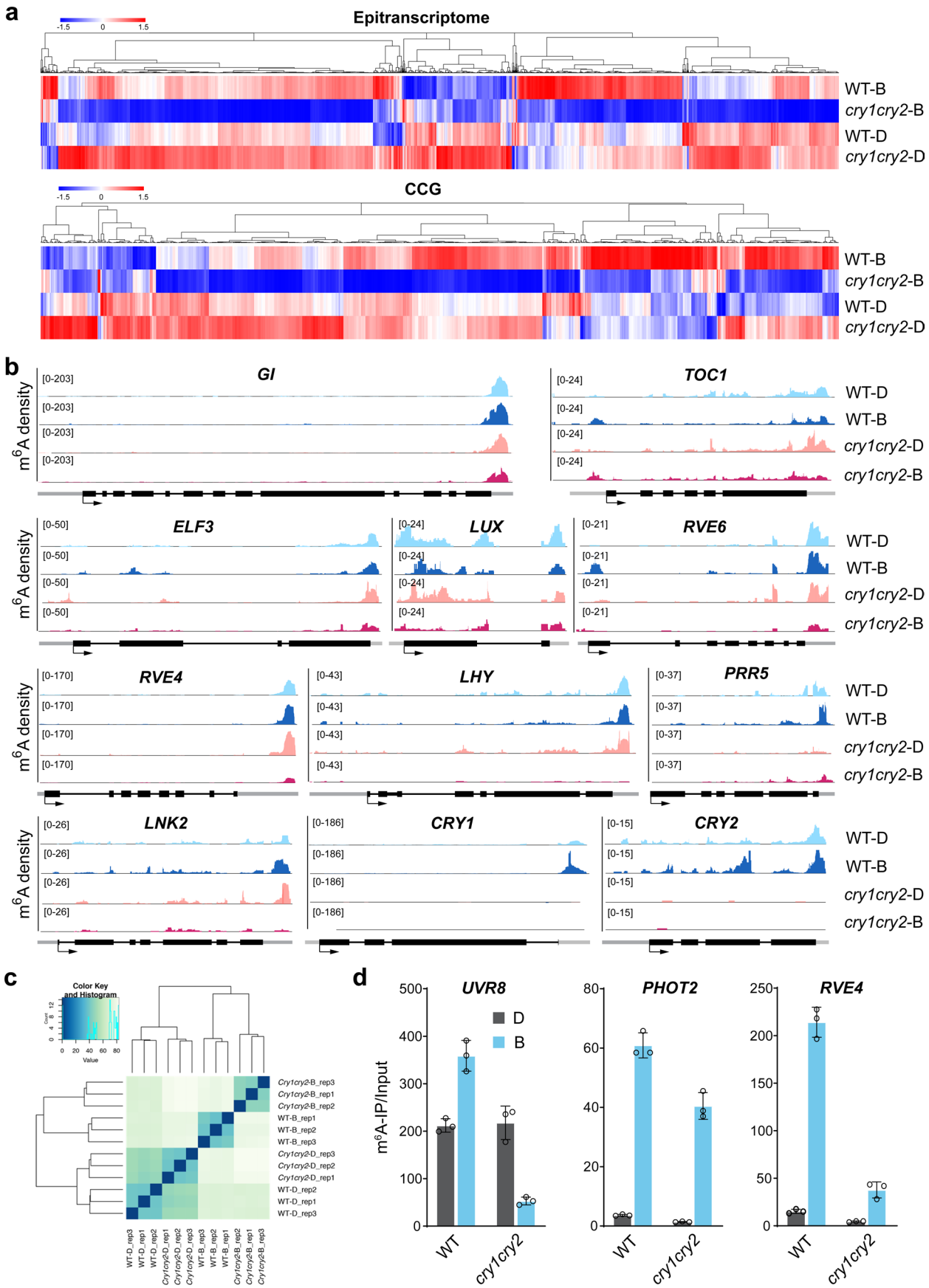

Extended Data Fig. 1 | See next page for caption.

Extended Data Fig. 1 | CRY-mediated photoresponsive epitranscriptomic changes in plants. a, The heatmaps showing relative m6A abundance for all genes (epitranscriptome, top) or clock-controlled genes (CCG, bottom) in wild type (WT) and cry1cry2 mutants grown in the dark (D) or blue light conditions (B). **b**, Genomic visualization of m6A density maps of core clock genes detected in m6A-seq. CRY1 and CRY2 detected only in WT but not cry1cry2 samples are shown as the negative control. **c**, Hierarchical clustering analysis of different m6A-seq samples indicates no unusual sample variances. **d**, m6A abundance of individual sites of selected genes was analyzed by m6A-IP-qPCR. The relative m6A level in each gene was calculated by normalizing the m6A-IP to input signals. Data are shown as Mean ± SD from 3 independent experiments. D, dark; B, blue light (30 μmol m-2 s-1).

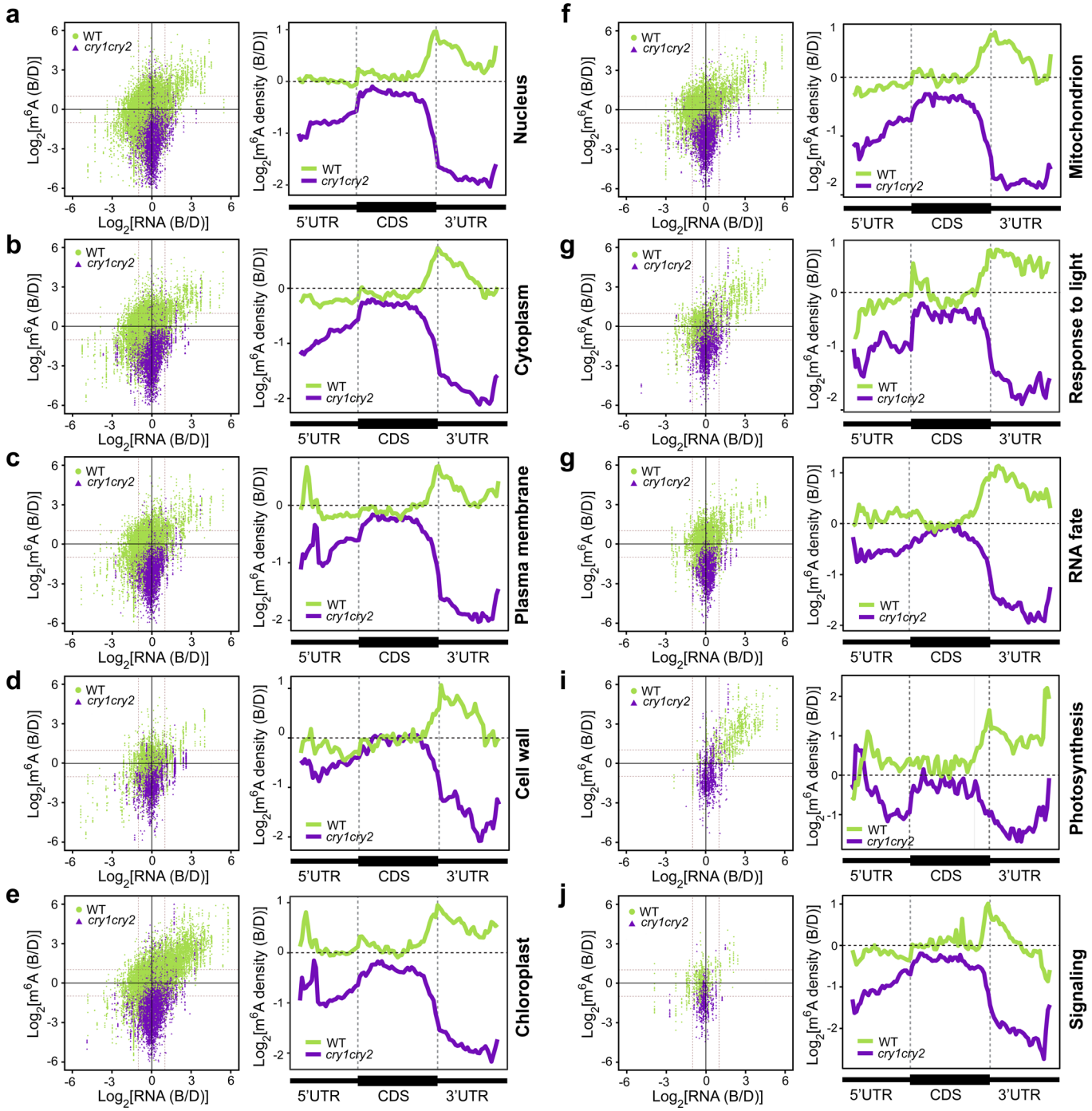

Extended Data Fig. 2 | Epitranscriptomes of selected GO group of genes. a–j, The scatter plots showing photoresponsive changes of m6A abundance and RNA abundance (left), and metagene profiles showing photoresponsive changes of m6A density (right) of mRNAs categorized as the TAIR10 GO groups.

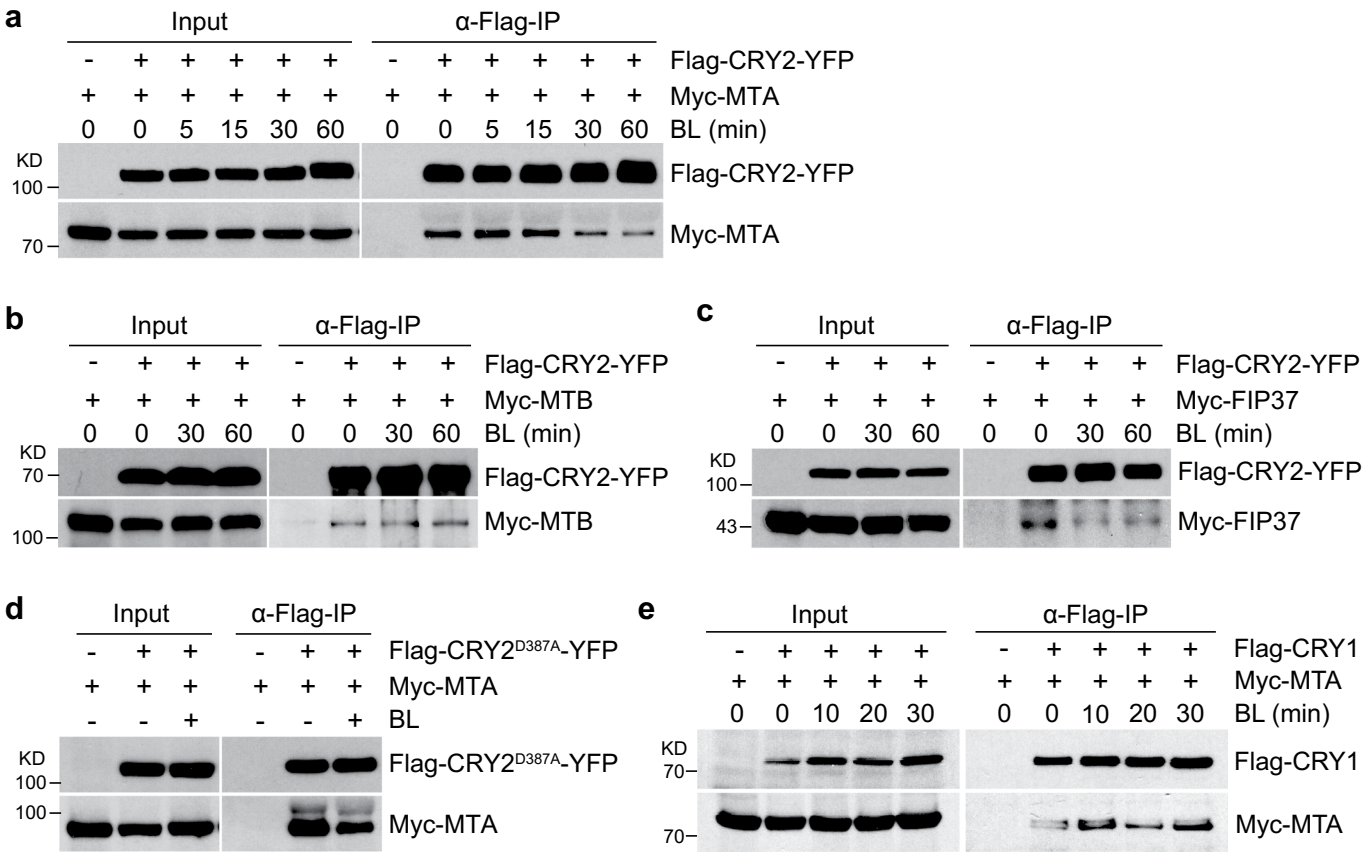

Extended Data Fig. 3 | CRYs interacts with subunits of m6A mRNA methyltransferase in human cells. a-c, co-IP assays showing interactions between CRY2 and MTA (a), MTB (b) and FIP37 (c) in HEK293T cells which were illuminated with blue light (BL; 100 μmol m-2 s-1) for indicated time (0-60 min). **d**, co-IP assay showing the interaction of CRY2D387A mutant and MTA in HEK293T cells with or without blue light irradiation. **e**, co-IP assay showing interactions between MTA and CRY1 in HEK293T cells. BL, blue light (100 μmol m-2 s-1). Three independent experiments are performed for a, two independent experiments for b-e, showing similar results.

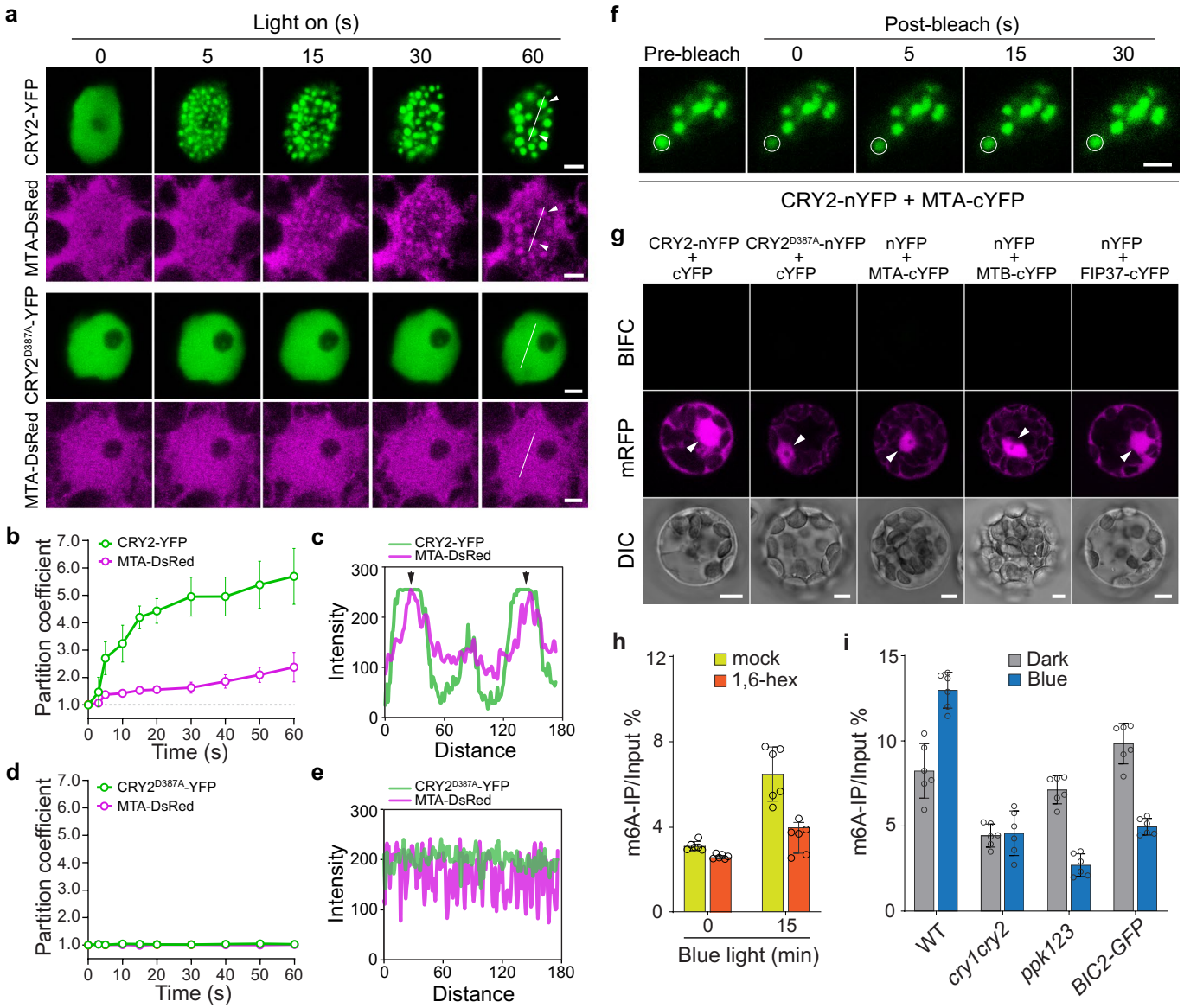

Extended Data Fig. 4 | Photoresponsive condensation of the CRY2-MTA complex in Arabidopsis. a, Time-lapse images showing the partial colocalization of MTA and CRY2 in CRY2 photobodies over the time of blue laser illumination in Arabidopsis protoplasts. Scale bar= 2 μm. Two independent experiments are performed showing similar results. **b**, Quantification of partition coefficient of CRY2-YFP and MTA-DsRed in the assay shown in (a). The data is presented as mean ± SD (n = 15 independent measurements from 5 nuclei). **c**, Fluorescence profiles of CRY2-YFP and MTA-DsRed over the white line shown in (a). The arrow heads indicate the locations of photobodies. **d**, Quantification of partition coefficient of CRY2D387A-YFP and MTA-DsRed in the assay shown in (a). The data is presented as mean ± SD (n = 15 independent measurements from 5 nuclei). **e**, Fluorescence profiles of CRY2D387A-YFP and MTA-DsRed over the white line shown in (a). f, FRAP of CRY2/MTA BiFC photobodies in protoplasts. White circle indicates the region for photobleaching. Quantification of FRAP is shown in Fig. 2m. Scale bar= 2 μm. g, Negative controls of BiFC assays. Plasmids expressing mRFP are used to monitor protoplasts transformation efficiency. The arrow in the cell indicates the location of nucleus. Scale bar = 5μm. Two independent experiments are performed showing similar results. h, m6A-IP-qPCR assay showing the relative abundance of m6A on the 3′UTR of CCA1 mRNA in etiolated wild-type seedlings treated with mock (H2O) or 1,6-hexanediol (10%) in response to blue light. The data is shown as Mean ± SD (n = 6 technical replicates from 2 biological repeats). i, m6A-IP-qPCR assay showing the relative abundance of m6A on the 3′UTR of CCA1 mRNA in wild-type (WT) and indicated genotypes grown in the Dark or Blue light (30 μmol m-2 s-1). The data is shown as Mean ± SD (n = 6 technical replicates from 2 biological repeats).

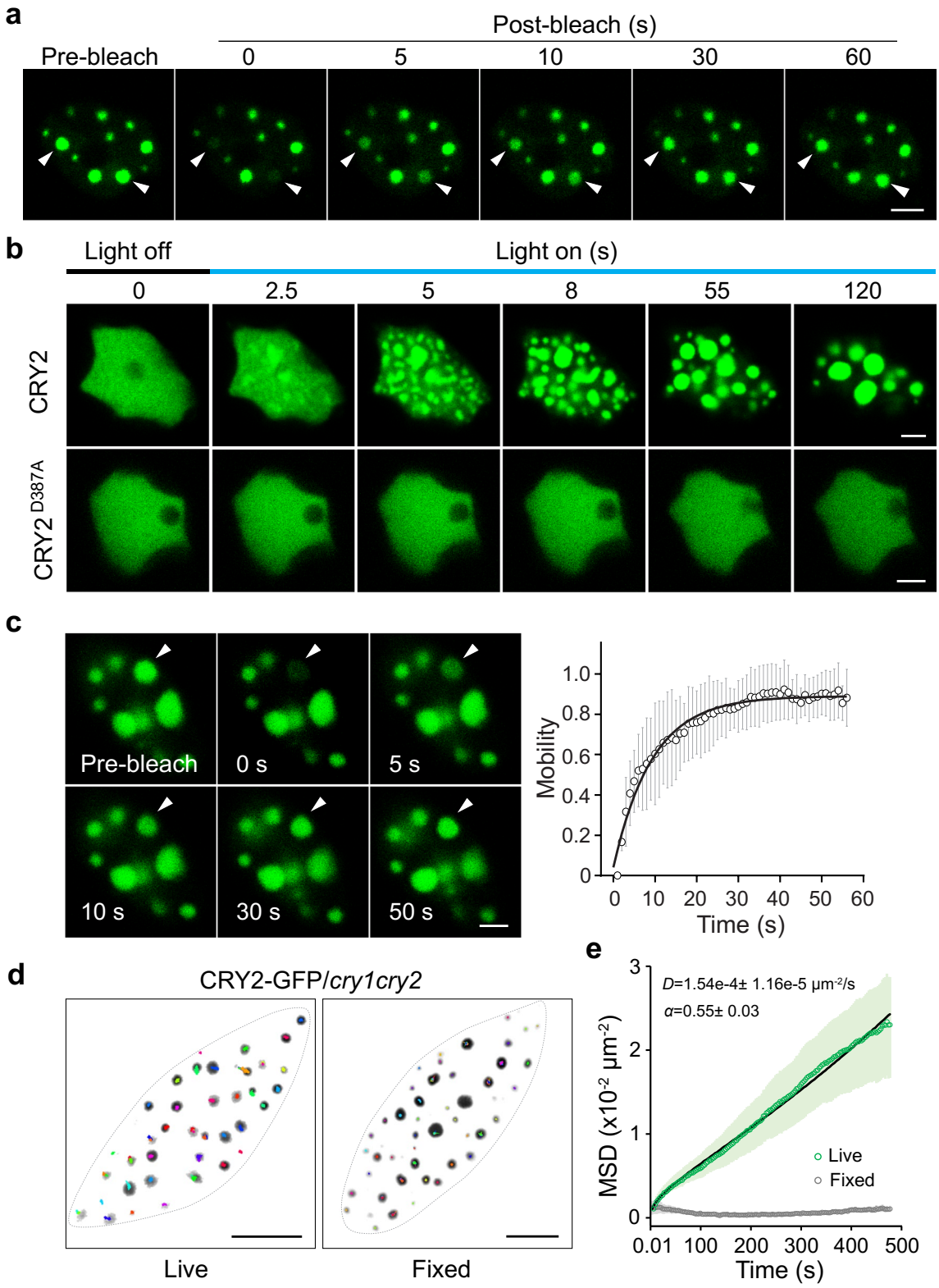

Extended Data Fig. 5 | See next page for caption.

Extended Data Fig. 5 | LLPS of CRY2 in plant cells. a, FRAP of CRY2 photobodies in CRY2-GFP transgenic plants, the quantification of FRAP is shown in Fig. 3c. Scale bar = 2μm. **b**, Time-lapse images showing light-elicited formation of CRY2-YFP photobodies in protoplasts. Light-insensitive CRY2D387A-YFP was used as the negative control. Quantification of partition coefficient for both CRY2-YFP and CRY2D387A-YFP fluorescence is shown in Fig. 3e. Scale bar = 2μm. **c**, FRAP of CRY2-YFP photobodies in Arabidopsis protoplasts. Protoplasts transfected with CRY2-YFP were illuminated with 488 nm laser for 30 s before FRAP. Time-lapse images before and after FRAP are shown on the left, white arrow heads point at the photobodies for photobleaching. Quantification of FRAP assay is shown on the right. Double exponential fit (the dark line) of normalized and averaged recovery curves is shown (n = 5 independent experiments; Mean ± SD). Scale bar = 2μm. **d**, Representative motion trajectories of CRY2-GFP photobodies in the live or fixed plant nucleus. The time-lapse images were taken every 3 s for 10 min. The dashed lines in the images are the outlines of the nucleus. Scale bar= 5 μm. **e**, The ensemble-averaged MSD (Mean Square Displacement) curves of tracked CRY2-GFP photobodies (as shown in d) in live or fixed samples. Shaded areas represent standard error (SE) of the mean (n = 4 and 3 independent cells for the live and fixed sample, respectively). Fitting of the MSD for live sample to the anomalous diffusion model yields the Diffusion constant (D), anomalous exponent (α; $\alpha < 1$ indicates the subdiffusive motion of the particles) and the best fitted curve (black line) which are shown in the graph.

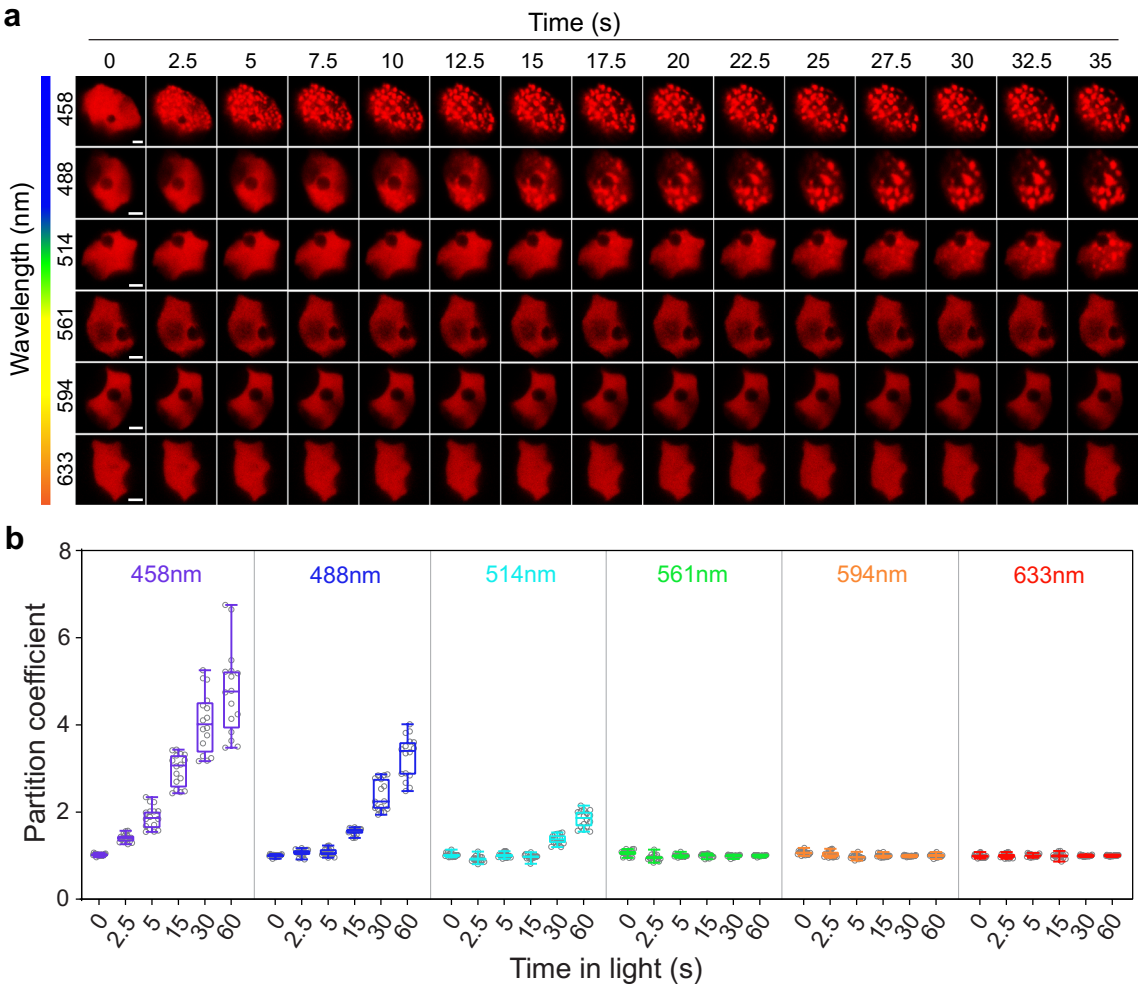

Extended Data Fig. 6 | Wavelength specificity of LLPS of CRY2-DsRed in Arabidopsis protoplasts. a, Time-lapse images showing CRY2-DsRed distribution pattern in the nucleus under different wavelengths in protoplasts. Protoplasts transiently expressing CRY2-DsRed were kept in the dark and illuminated with different lasers during imaging. Scale bar=2 μm. **b**, Quantification of PC of CRY2-DsRed under different wavelengths (n = 16 measurements for each time point from 3 nuclei; in each box, the center line denotes median value; boxes extend from the 25th to the 75th percentile of each group's distribution of values; vertical extending lines denote the range from minima to maxima; the open circles denote the values ranging from minima to maxima).

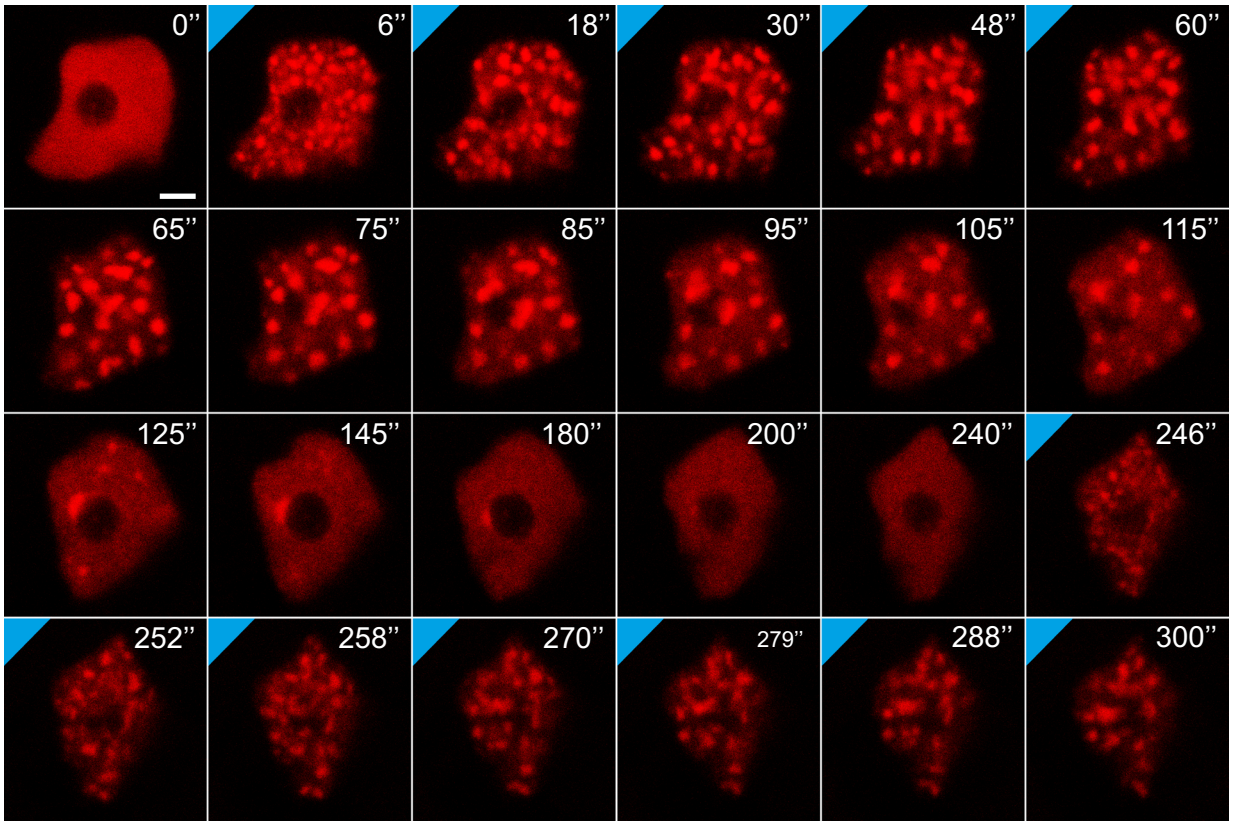

Extended Data Fig. 7 | CRY2 photobodies are reversible in response to light-dark cycles in Arabidopsis protoplasts. Time-lapse images of CRY2-DsRed expressed in protoplasts. Blue triangle indicates that 488 nm laser was on during imaging. Quantification of this experiment is shown in Fig. 3d. Scale bar=2 μm.

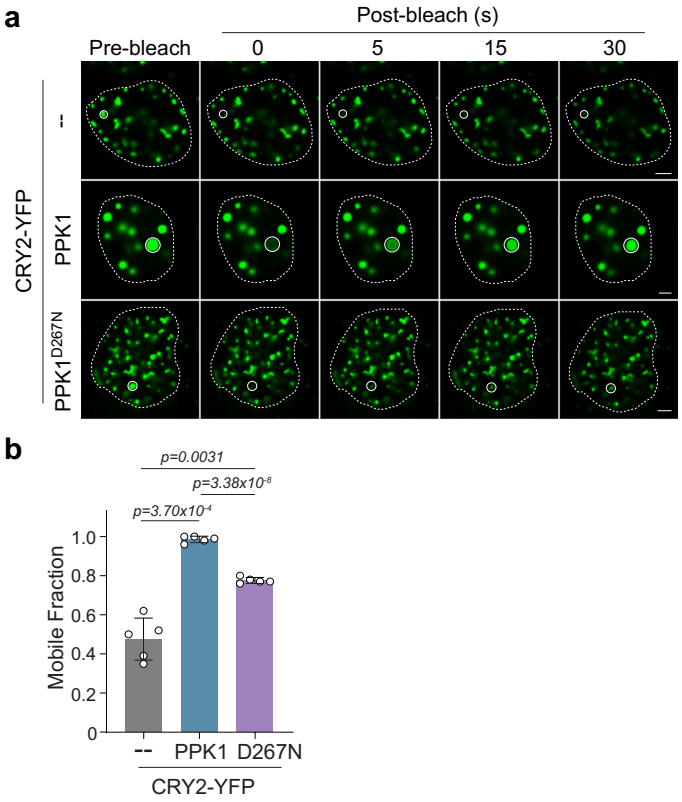

Extended Data Fig. 8 | PPK1-dependent phosphorylation is essential to maintain CRY2 photobodies in liquid phase. a, Representative images showing the FRAP of CRY2 photobody in HEK293T cells with or without co-expression of PPK1 or PPK1D267N. The quantification of FRAP assays is shown in Fig. 3j. The dashed circle outlines the nucleus and the small solid circle inside the nucleus indicates the region for photobleaching. Scale bar = 2μm. **b**, The mobile fraction of CRY2 photobodies at 57 s after photobleaching (mean ± SD; n = 5 independent experiments). p value is calculated in two-tailed Students' t-test.

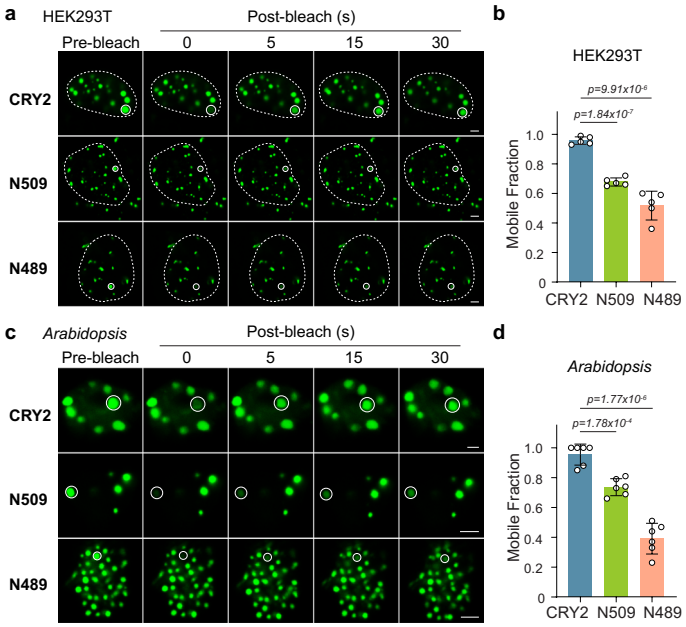

Extended Data Fig. 9 | C-terminus of CRY2 is necessary to maintain the photobodies in liquid phase in both human cells and Arabidopsis protoplasts. a, Representative images showing the FRAP of CRY2, CRY2N509 (N509) and CRY2N489 (N489) photobodies in the presence of PPK1 in HEK293T cells. The dashed circle outlines the nucleus and the small solid circle inside the nucleus indicates the region for photobleaching. The quantification of FRAP assays is shown in Fig. 3m. Scale bar = 2μm. b, The mobile fraction of CRY2, N509 and N489 photobodies at 57 s after photobleaching in HEK293T cells (mean ± SD; n = 5 independent experiments). p value is calculated in two-tailed Students' t-test. c, Images showing the FRAP of CRY2, N509 and N489 photobodies in Arabidopsis protoplasts. The circle inside the nucleus indicates the region for photobleaching. The quantification of FRAP assays is shown in Fig. 3n. Scale bar = 2μm. d, The mobile fraction of CRY2, N509 and N489 photobodies at 57 s after photobleaching in protoplasts (mean ± SD; n = 6 independent experiments). p value is calculated in two-tailed Students' t-test.

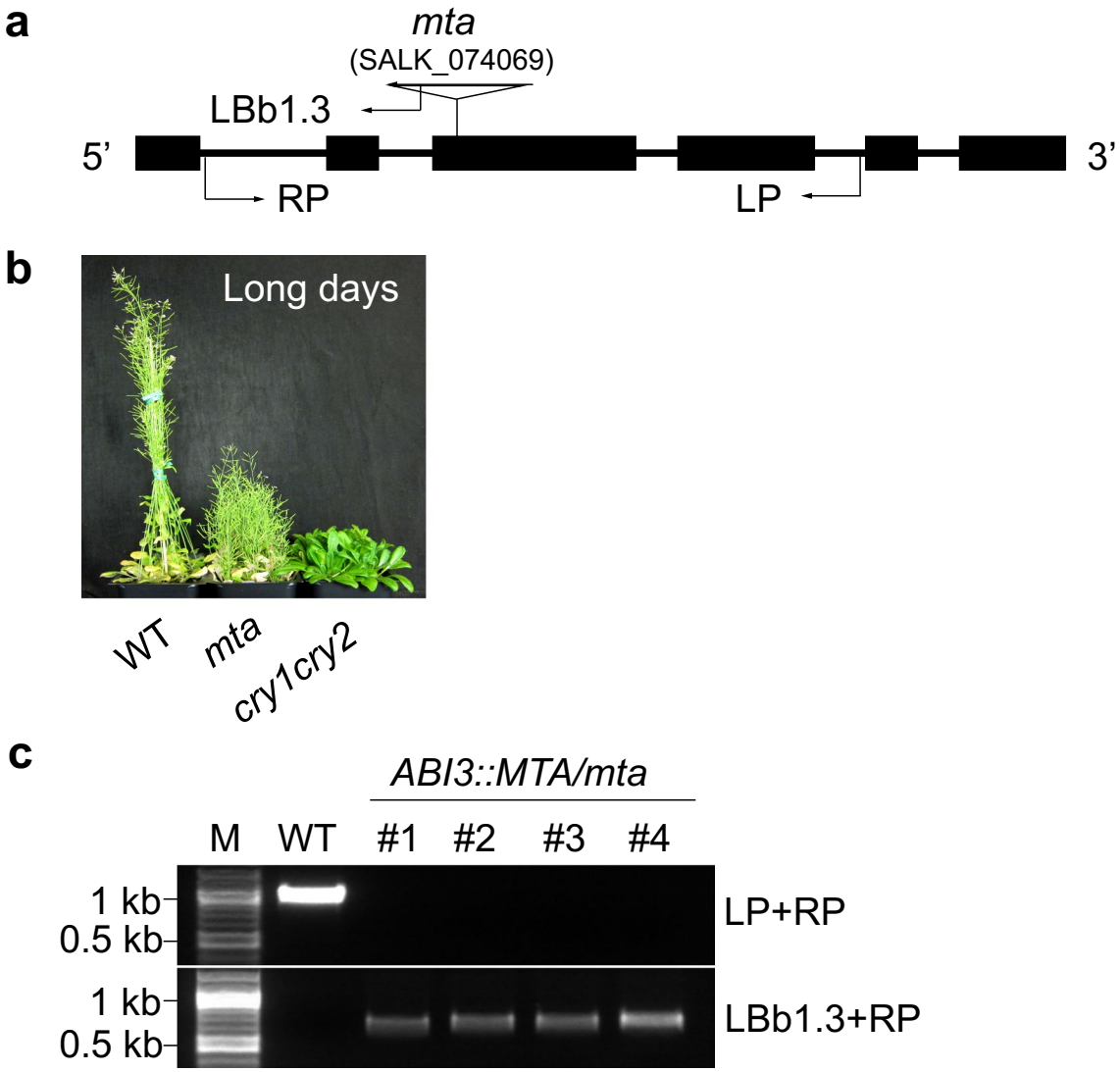

Extended Data Fig. 10 | Genotyping of ABI3::MTA/mta plants. a, The schematic diagram of the T-DNA insertion mta mutant (SALK_074069). The exons (boxes), introns (lines) of the MTA gene and the T-DNA insert (opened triangle) are shown. The positions of primers used for genotyping the mutant locus are marked on MTA gene structure. The positions of RP (right primer) or LP (left primer) of the MTA gene, and primer LBb1.3 in the left border of T-DNA insert are indicated. b, Representative image of WT, mta (short for ABI3::MTA/mta) and cry1cry2 plants grown in long day conditions for 50 days. c, Genomic PCR of the MTA locus in WT and ABI3::MTA/mta plants using genomic DNA as the templates. The sizes of the PCR products were 965 bp (amplified with LP + RP) or 444-744 bp (amplified with LBb1.3+RP). Four plants (#1-#4) were randomly selected from a ABI3::MTA/mta population for genotyping. M, DNA marker.

nature research

Corresponding author(s): Qin Wang and Chentao Lin

Last updated by author(s): Jul 12, 2021

Reporting Summary

Nature Research wishes to improve the reproducibility of the work that we publish. This form provides structure for consistency and transparency in reporting. For further information on Nature Research policies, see our Editorial Policies and the Editorial Policy Checklist.

Statistics

For all statistical analyses, confirm that the following items are present in the figure legend, table legend, main text, or Methods section.

n/a	Confirmed	
☐	☒	The exact sample size (*n*) for each experimental group/condition, given as a discrete number and unit of measurement
☐	☒	A statement on whether measurements were taken from distinct samples or whether the same sample was measured repeatedly
☐	☒	The statistical test(s) used AND whether they are one- or two-sided *Only common tests should be described solely by name; describe more complex techniques in the Methods section.*
☒	☐	A description of all covariates tested
☒	☐	A description of any assumptions or corrections, such as tests of normality and adjustment for multiple comparisons
☐	☒	A full description of the statistical parameters including central tendency (e.g. means) or other basic estimates (e.g. regression coefficient) AND variation (e.g. standard deviation) or associated estimates of uncertainty (e.g. confidence intervals)
☐	☒	For null hypothesis testing, the test statistic (e.g. *F*, *t*, *r*) with confidence intervals, effect sizes, degrees of freedom and *P* value noted *Give P values as exact values whenever suitable.*
☒	☐	For Bayesian analysis, information on the choice of priors and Markov chain Monte Carlo settings
☒	☐	For hierarchical and complex designs, identification of the appropriate level for tests and full reporting of outcomes
☐	☒	Estimates of effect sizes (e.g. Cohen's *d*, Pearson's *r*), indicating how they were calculated

Our web collection on statistics for biologists contains articles on many of the points above.

Software and code

Policy information about availability of computer code

Data collection	ZEN 3.0 software accompanied with ZEISS LSM 780 was used to acquire the microscopic images used in this study;
Data analysis	FIJI/ImageJ 1.53c was used for microscopic images analysis; GraphPad Prism 8.0.2 was used for statistical analysis; easyFRAP software was used for FRAP data analysis; FASTX-toolkit v0.0.13, TopHat v2.0.11 and SAMtools-1.12 were used for RNA-seq and m6A-seq data analysis;

For manuscripts utilizing custom algorithms or software that are central to the research but not yet described in published literature, software must be made available to editors and reviewers. We strongly encourage code deposition in a community repository (e.g. GitHub). See the Nature Research guidelines for submitting code & software for further information.

Data

Policy information about availability of data

All manuscripts must include a data availability statement. This statement should provide the following information, where applicable:

- Accession codes, unique identifiers, or web links for publicly available datasets
- A list of figures that have associated raw data
- A description of any restrictions on data availability

All data supporting the findings of this study are available in the Source Data or the Supplementary Table. Biological materials used in this study are available from the corresponding author (Chentao Lin) on reasonable request. RNA-seq and m6A-seq raw data (associated with Fig.1 and Extended Data Fig. 1-2) were deposited in the NCBI Gene Expression Omnibus under accession number GSE152466 which has been released on July 12th, 2021.

Field-specific reporting

Please select the one below that is the best fit for your research. If you are not sure, read the appropriate sections before making your selection.

☒ Life sciences ☐ Behavioural & social sciences ☐ Ecological, evolutionary & environmental sciences

For a reference copy of the document with all sections, see nature.com/documents/nr-reporting-summary-flat.pdf

Life sciences study design

All studies must disclose on these points even when the disclosure is negative.

Sample size	No statistical methods were used to predetermine sample sizes. Required experimental sample sizes were estimated based on previous established protocols in the field (https://doi.org/10.1007/978-1-0716-1370-2). The sample sizes were adequate as the experimental results were reproducible.
Data exclusions	No data were excluded from the analysis
Replication	All experimental findings were reproduced in several independent biological experiments (N) with multiple technical replicates. The number of repeats is indicated in the figure legends.
Randomization	Samples of the same genotypes were randomly collected and pooled for downstream experiments.
Blinding	Blinding was not possible as the authors who performed the experiments also analyzed the data.

Reporting for specific materials, systems and methods

We require information from authors about some types of materials, experimental systems and methods used in many studies. Here, indicate whether each material, system or method listed is relevant to your study. If you are not sure if a list item applies to your research, read the appropriate section before selecting a response.

Materials & experimental systems

n/a	Involved in the study
☐	☒ Antibodies
☐	☒ Eukaryotic cell lines
☒	☐ Palaeontology and archaeology
☒	☐ Animals and other organisms
☒	☐ Human research participants
☒	☐ Clinical data
☒	☐ Dual use research of concern

Methods

n/a	Involved in the study
☒	☐ ChIP-seq
☒	☐ Flow cytometry
☒	☐ MRI-based neuroimaging

Antibodies

Antibodies used	anti-CRY2 antibody is prepared in our lab (Ref: Science. 1998. 279:1360-1363; dilution 1:3,000) , anti-FLAG antibody (Cat.# F3165, Sigma; dilution 1:3,000), anti-Myc antibody (Cat.# 05-724, Millipore; dilution 1:3,000), anti-GFP antibody (B-2, Cat.# sc-9996, Santa Cruz Biotechnology; dilution 1:3,000) and anti-m6A antibody (Cat.#: 202003, Synaptic Systems; dilution 1: 50)
Validation	Validation of anti-CRY2 antibodies was described in the reference: Science. 1998. 279:1360-1363; validation of all the other commercial antibodies could be found on the manufacturers' websites: for anti-FLAG antibody (https://www.sigmaaldrich.com/catalog/product/sigma/f3165?lang=en&region=US); for anti-Myc antibody (https://www.emdmillipore.com/US/en/product/Anti-Myc-Tag-Antibody-clone-4A6,MM_NF-05-724); for anti-GFP antibody (https://www.scbt.com/p/gfp-antibody-b-2?gclid=EAIaIQobChMIsZzsrJKg6gIVcgnnCh05QgAPEAAYASAAEgKvA_D_BwE); for anti-m6A antibody (https://sysy.com/product/202003)

Eukaryotic cell lines

Policy information about cell lines

Cell line source(s)	Human embryo kidney cells (HEK293T) is botained from ATCC (https://www.atcc.org/products/crl-3216#:~:text=The%20293T%20cell%20line%2C%20originally,the%20SV40%20region%20of%20replication.)
Authentication	The HEK293T cell line used in this study is not authenticated
Mycoplasma contamination	The HEK293T cell line used in this study was not specifically tested for Mycoplasma contamination. However, no abnormalities of cultured cells have been observed, such as slowed cell growth and interfered cell attachment.

Commonly misidentified lines (See ICLAC register)	no commonly misidentified cell lines were used in the study